WATER RESOURCES RESEARCH, VOL. 49, 5501–5519, doi:10.1002/wrcr.20405, 2013

# Interpreting streamflow generation mechanisms from integrated surface-subsurface flow models of a riparian wetland and catchment

D. Partington,[1] P. Brunner,[2] S. Frei,[3] C. T. Simmons,[4] A. D. Werner,[4] R. Therrien,[5] H. R. Maier,[1] G. C. Dandy,[1] and J. H. Fleckenstein[6]

Received 9 November 2012; revised 15 May 2013; accepted 7 July 2013; published 9 September 2013.

[1] The understanding of streamflow generation processes is vitally important in the management of water resources. In the absence of the data required to achieve this, Integrated Surface-Subsurface Hydrological Models (ISSHM) can be used to assist with the development of this understanding. However, the standard outputs from these models only enable elicitation of information about hydrological drivers and hydrological responses that occur at the same time. This generally limits the applicability of ISSHMs for the purposes of obtaining an improved understanding of streamflow generation processes to catchment areas that do not exhibit significant storage, travel times or flow depletion mechanisms. In order to overcome this limitation, a previously published Hydraulic Mixing-Cell (HMC) method is improved so that it can be used to follow surface water derived from direct rainfall and groundwater discharge to the stream and adjacent overland flow areas. The developed approach was applied to virtual experiments (based on the Lehstenbach catchment in southeastern Germany), which are composed of two ISSHMs of contrasting scales: (1) a riparian wetland of area 210 $m^2$ and (2) a catchment of area 4.2 $km^2$. For the two models, analysis of modeling results for a large storm event showed complex spatiotemporal variability in streamflow generation and surface water-groundwater interaction. Further analysis with the HMC method elucidated in-stream and overland flow generation mechanisms. This study showed within a modeling framework that identification and quantification of in-stream and overland flow generation better informed understanding of catchment functioning through decomposition of streamflow hydrographs, and analysis of spatiotemporal variability of flow generation mechanisms.

**Citation:** Partington, D., P. Brunner, S. Frei, C. T. Simmons, A. D. Werner, R. Therrien, H. R. Maier, G. C. Dandy, and J. H. Fleckenstein (2013), Interpreting streamflow generation mechanisms from integrated surface-subsurface flow models of a riparian wetland and catchment, *Water Resour. Res.*, *49*, 5501–5519, doi:10.1002/wrcr.20405.

## 1. Introduction

[2] Understanding streamflow generation and surface water-groundwater interaction is of great importance for the management of water resources, as highlighted in reviews by *Winter* [1999], *Sophocleous* [2002], and more recently *Fleckenstein et al*. [2010]. In the absence of relevant data, distributed physics-based Integrated Surface-Subsurface Hydrological Models (ISSHM) [see *Gaukroger and Werner*, 2011; *Sebben et al*., 2013] represent a useful alternative for providing insight into hydrological processes at detailed spatiotemporal resolutions [e.g., *Mirus et al*., 2011b]. This is because ISSHMs are capable of simulating feedbacks between the surface and subsurface, including all forms of overland flow generation and reinfiltration [*Kampf and Burges*, 2007]. In addition, ISSHMs can assist with analyzing and interpreting hydrological processes and in developing conceptual understanding of catchment processes [*Ebel and Loague*, 2006]. ISSHM examples include HydroGeoSphere [*Therrien et al*., 2009], InHM [*Vanderkwaak*, 1999], ParFLOW [*Kollet and Maxwell*, 2006], CATHY [*Camporese et al*., 2010], and MODHMS [*HydroGeoLogic Inc*., 2006]. In recent years, studies related to understanding streamflow generation and surface water-groundwater interaction using numerical models have become increasingly widespread [e.g., *Brunner et al*., 2009; *Frei et al*., 2010; *Maxwell and Kollet*, 2008; *Park et al*., 2011].

[1]School of Civil, Environmental and Mining Engineering, University of Adelaide, Adelaide, South Australia, Australia.
[2]Centre of Hydrogeology and Geothermics, Neuchâtel, Switzerland.
[3]Department of Hydrology, University of Bayreuth, Bayreuth, Germany.
[4]School of the Environment and National Centre for Groundwater Research and Training, Flinders University, Adelaide, South Australia, Australia.
[5]Department of Geology and Geological Engineering, Université Laval, Quebec, Quebec, Canada.
[6]Department of Hydrogeology, Helmholtz-Center for Environmental Research-UFZ, Leipzig, Germany.

Corresponding author: D. Partington, School of Civil, Environmental and Mining Engineering, University of Adelaide, Adelaide, SA 5005, Australia. (daniel.partington@adelaide.edu.au)

©2013. American Geophysical Union. All Rights Reserved.
0043-1397/13/10.1002/wrcr.20405

[3] The aforementioned studies focused on processes in small-scale synthetic systems, enabling insight to be gained into the controls on flow generation [*Frei et al*., 2010; *Maxwell and Kollet*, 2008; *Park et al*., 2011] and depletion [*Brunner et al*., 2009]. However, difficulties arise when attempting to gain the same level of insight for larger, catchment-scale systems. This is because in small-scale systems, hydrological outputs at a particular place and time are generally only affected by hydrological drivers that occur at the same location and at the same time (i.e., by "active" processes [*Ambroise*, 2004]). However, this is not the case for larger-scale systems, where local hydrologic response is not only affected by local processes but also largely by processes taking place in other locations and at other times. This is a result of the influence of surface and groundwater flow travel times, flow impediments (e.g., riparian wetlands or weirs), and losses (e.g., infiltration or evaporation). Consequently, hydrological drivers that occur at a particular point in time (active processes) do not necessarily end up contributing to the hydrological output at that or a later time. As a result, when considering streamflow generation processes at the catchment scale, there is a need to distinguish between "active" and "contributing" processes [*Ambroise*, 2004], where contributing processes are those that contribute to flow at a particular location at a particular time, and necessarily include active processes upstream of the point of interest. It follows therefore that all contributing processes are derived from active processes, occurring both upstream and at the point of interest; however, not all active processes will become contributing processes downstream of where they occur, due to flow depletion processes such as evapotranspiration, and infiltration to the subsurface. This distinction is particularly important in catchments with relatively long travel times for water and/or where flow depletion processes are significant.

[4] While information on active processes is provided as standard output from ISSHMs, the same is not the case for information on contributing processes. For example, the lag times between individual recharge events and resulting stream flow increases are not reported. As a result, previous studies that have used ISSHMs at the catchment scale [e.g., *Goderniaux et al*., 2009, 2011; *Loague and Vanderkwaak*, 2002; *Ebel et al*., 2008; *Li et al*., 2008; *Shen and Phanikumar*, 2010; *Mirus et al*., 2011a; *Camporese* et al., 2010] have been unable to identify and quantify the individual contributions of various catchment processes to streamflow generation processes. Although *Vivoni et al*. [2007] quantified the contributing processes of streamflow generation at the catchment scale, their model was based on a number of simplifying assumptions that did not necessitate the distinction between active and contributing processes. In particular, they assumed that surface water flows to the catchment outlet without loss or impediment once it enters the surface domain [see *Ivanov et al*., 2004]. This assumption is problematic in more complex systems where significant fractions of overland and in-stream flows are depleted (e.g., due to reinfiltration of overland flow on the hillslope, or losing sections along a stream) or retained in particular parts of the catchment (e.g., due to wetlands, weirs, or other flow impediments and water storages).

[5] In order to enable ISSHMs to be used for the identification of both active and contributing streamflow generating processes, it is necessary to first classify water as it enters the surface by the active flow generation mechanism, and then track that water on its journey through the catchment, to the point at which the hydrograph is being measured. *Partington et al*. [2011, 2012] and *Li et al*. [2013] achieved this by developing and applying a Hydraulic Mixing-Cell (HMC) method in order to identify the groundwater discharge components of hydrographs for a relatively flat synthetic catchment that exhibited dynamic gaining and losing reaches along the stream, and furthermore displayed clear time lags for flow from upstream areas. However, this approach has not yet been applied to larger-scale catchments, or for the identification of overland flow generation mechanisms.

[6] In this paper, the HMC method introduced by *Partington et al*. [2011] is modified to enable information about active and contributing processes to be obtained as outputs from ISSHMs. This enables the identification and quantification of contributing in-stream and overland flow generation mechanisms at larger (e.g., catchment) scales which informs the understanding of catchment functioning. This is particularly important as there are still difficulties in the capability to conduct or scale up the measurements of active processes that are required in order to gain an understanding of surface water-groundwater interactions and streamflow generation at the catchment scale [*Fleckenstein et al*., 2010]. The Lehstenbach catchment is used as the basis for virtual experiments with the modified HMC method. Two models of contrasting scales are used to investigate both in-stream and overland flow generation mechanisms within the catchment. In-stream flow generation mechanisms are defined as those occurring on the boundaries of the stream, i.e., direct precipitation to the stream, direct groundwater discharge to the stream and overland flow into the stream. Overland flow generation is distinguished by rainfall runoff from the hillslope (without distinguishing infiltration excess and saturation excess) and groundwater discharge on the hillslope adjacent to the stream. Using the HMC method, this paper aims to demonstrate the value of quantifying in-stream and overland flow generation mechanisms to better understand processes at the catchment scale within the virtual experiments by:

[7] 1. Separating flow hydrographs into the constituent in-stream and overland flow generation mechanisms at the outlet and other select points;

[8] 2. Quantifying the spatial and temporal variability for in-stream and overland flow generation mechanisms at contrasting spatial (wetland 210 $m^2$ and catchment 4.2 $km^2$) and temporal (days versus year) scales; and

[9] 3. Quantifying the differences between active and contributing processes within the catchment.

## 2. Case Study: Lehstenbach Catchment

[10] The Lehstenbach catchment, (4.2 $km^2$) located in Southeastern Germany (50°8′35″N, 11°52′8″E, see Figure 1), has been the subject of a number of previous studies [*Lischeid et al*., 2002, 2007; *Frei et al*., 2010]. Elevations within the catchment vary between 877 m above sea level in upslope areas and 690 m above sea level at the catchment's outlet. Average annual precipitation amounts to about 1150 mm/yr, the average annual evapotranspiration is

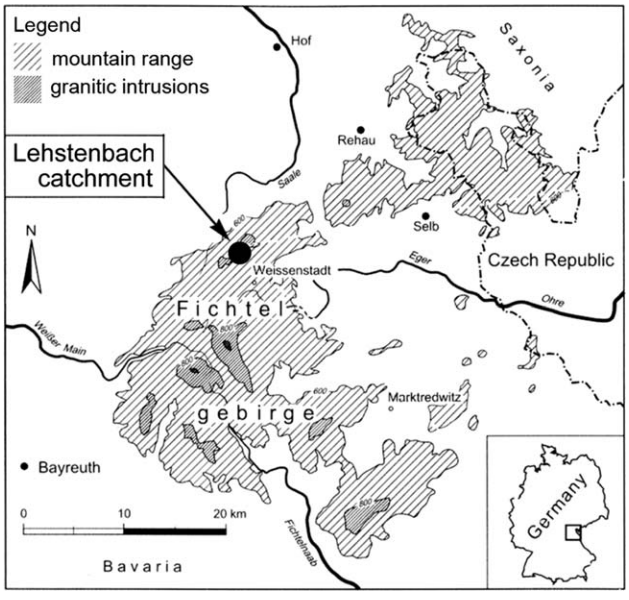


**Figure 1.** Location of the Lehstenbach catchment (after *Frei et al*., [2010]).

approximately 600 mm/yr, and average annual runoff from the catchment is approximately 550 mm/yr [*Gerstberger*, 2001]. The annual mean air temperature is approximately 5°C [*Gerstberger*, 2001].

[11] The main regional aquifer in the Lehstenbach catchment is made of regolith material (around 40 m thick) originating from the weathering of the granitic bedrock [*Lischeid et al*., 2002]. Nearly one third of the catchment's total area can be classified as riparian wetlands, adjacent to the major streams. These wetlands are preferentially located in the center of the bowl-shaped catchment, where subsurface flows converge. Within the wetland areas, groundwater levels typically fluctuate within the uppermost 0.5 m of the organic peat soil. In the upslope areas, which are mainly forested (*Picea abies*), groundwater levels are generally between 5 and 10 m below the surface. Locally, the hydraulic connectivity between the groundwater in the riparian wetlands and the deeper regolith aquifer is restricted by an up to 2 m thick basal clay layer.

[12] Previous studies of the Lehstenbach catchment indicated that the dominant runoff generation processes (e.g., saturated overland flow and shallow subsurface flow) during rainfall events take place within the wetland areas [*Lischeid et al*., 2007; *Frei et al*., 2010]. Large areas of these wetlands, predominantly located near the catchment's outlet, are characterized by a pronounced microtopography, consisting of sequences of hollows and hummocks formed by the wetland's vegetation [*Knorr et al*. 2008]. A conceptual hillslope plot depicting the in-stream and overland flow generation mechanisms in the Lehstenbach catchment is shown in Figure 2.

[13] Previous modeling by *Frei et al*. [2010, 2012] has been carried out for a synthetic riparian wetland typical of those within the Lehstenbach catchment. *Frei et al*. [2010] demonstrated a hysteretic relationship between wetland water storage and channel discharge. They concluded that enhanced mixing between surface and subsurface water had potential implications for the water quality within the catchment. However, *Frei et al*. [2010] did not explore mixing of rainfall and discharged groundwater at the wetland's surface, which necessitates quantifying the different overland surface flow and ponding generation mechanisms. These complex processes in the wetland suggest an analysis of only the active mechanisms is insufficient to quantify the contributing overland flow generation mechanisms. In the present study, application of the HMC method to the wetland model expands on the work of *Frei et al*. [2010] and is used to quantify the fractions of overland flow that are generated from either rainfall running off the wetland or groundwater discharging to the wetland. However, their wetland model does not include the surrounding influences of adjacent wetlands, upslope forested areas, and groundwater flows from upslope and deeper aquifers within the catchment. To investigate the catchment-scale processes, a model of the entire Lehstenbach catchment is developed, allowing analysis of in-stream and overland flow generation across the entire stream network and catchment, as well as accounting for contributions to the wetlands from deeper groundwater that originated from upslope areas.

## 3. Methodology

[14] The modeling investigation within the study area is carried out at two different scales, as mentioned previously. First, the model of a synthetic wetland typical of those in the Lehstenbach catchment is revisited, following *Frei et al*. [2010] (section 3.2.1). Second, a model of the entire Lehstenbach catchment is developed (section 3.2.2). In-stream and overland flow generation is analyzed using an improved HMC method detailed in section 3.3.

### 3.1. The Fully Integrated Modeling Platform

[15] Numerical modeling in this study uses the ISSHM HydroGeoSphere (HGS). HGS is a fully integrated surface-

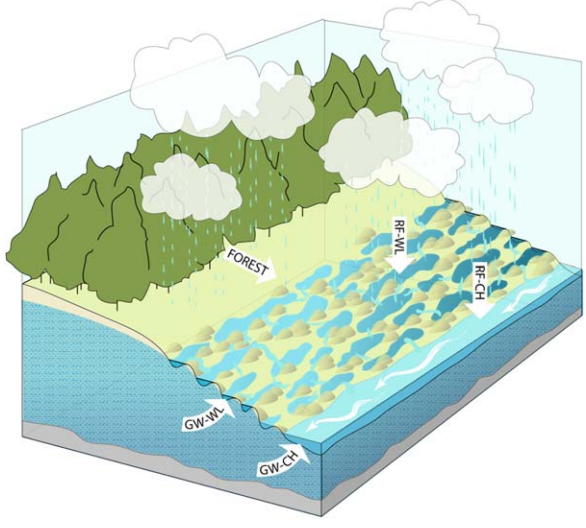


**Figure 2.** Conceptual diagram of in-stream and overland flow generation mechanisms typical of the Lehstenbach catchment during intense storm events. The in-stream and overland flow generation mechanisms shown are groundwater discharge to the channel (GW-CH) and wetland surfaces (GW-WL), direct rainfall to the channel (RF-CH) and wetland surfaces (RF-WL), and runoff from the forest.

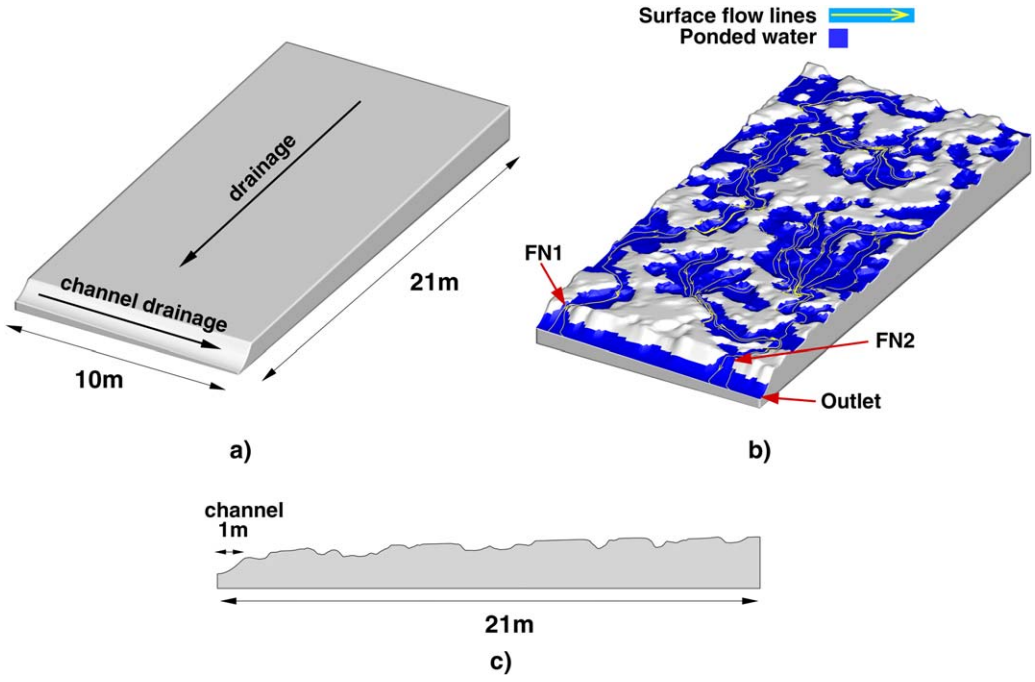


**Figure 3.** Geometry of the wetland segment: (a) planar reference model showing the main drainage direction and channel location; (b) smoothed realization of the wetland's hummocky microtopography, with simulation results of developed overland flow in the wetland [after *Frei et al*., 2010]; and (c) cross section ($Y = 5$ m) of the microtopography model [after *Frei et al*., 2010]. The division of overland flow into two distinct flow networks (denoted as FN1 and FN2) is shown by the surface flow lines. The model observation points for flow in this study are denoted by the red arrows, which correspond to surface water discharge from the wetlands to the channel from FN1 and FN2, and channel discharge at the outlet of the model.

subsurface flow model that incorporates 3-D variably saturated subsurface flow using a modified form of the Richard's equation and 2-D surface flow using the diffusion wave approximation to the St Venant equations. Further details of the numerical formulation of HGS can be found in *Therrien et al*. [2009] and *Brunner and Simmons* [2012]. The surface and subsurface are coupled using a first-order exchange coefficient [*Liggett et al*., 2012]. An important characteristic of fully integrated models such as HGS is that there is no requirement for a priori assumptions of specific streamflow generation mechanisms [*Mirus et al*., 2011a]. Consequently, it is necessary to interrogate the model outputs to characterize the streamflow generation processes that are predicted by the model.

### 3.2. Development of Case Study Models

#### 3.2.1. Wetland Model Setup

[16] The wetland model setup is described by *Frei et al*. [2010], and so only a brief description is presented here. The wetland model (Figure 3) is at the plot scale (21 m × 10 m), representing a relatively flat hillslope (average slope of 0.03 m/m) made up of a sequence of hummocks and hollows. The spatial structure of the microtopography is represented using geostatistical indicator simulations based on a Markov Chain model of transition probabilities [*Carle and Fogg*, 1996]. The model domain is made up of 10 layers, with a total of 410,832 elements and 210,000 nodes, providing a fine discretization of 0.1 m in the $X$, $Y$, and $Z$ directions. The organic peat is represented as homogeneous and isotropic with a saturated hydraulic conductivity of 0.2 m/d, a value that is based on a previous modeling study from the field site [*Hauck*, 1999] and which is in line with values reported for similar wetlands [*Kruse et al*., 2008; *Schlotzhauer and Price*, 1999]. Constitutive relationships for unsaturated flow are assumed to follow the van Genuchten model of the soil-water retention and relative permeability functions [*van Genuchten*, 1980]. The parameterization of the van Genuchten model is based on field measurements from similar wetlands located in Alberta, Canada [*Price et al*., 2010].

[17] *Frei et al*. [2010] showed that the pronounced microtopography resulted in distinct flow networks in the wetland model as shown in Figure 3b. The division of two flow networks (denoted as FN1 and FN2) and their discharge points to the channel are shown in Figure 3b.

[18] The simulation period in this study focuses on a large storm event (13–21 July 2001) from the 2000 to 2001 hydrological year (1 November 2000 to 31 October 2001). The simulation starts with a recession period (i.e., no rain) lasting 14 days. After day 14, an extended rainfall event occurs. The rainfall event persists for 8 days leading to the depressions on the slope filling until they spill to the adjacent down-slope depressions. Details of this "fill and spill" mechanism [after *Tromp-van Meerveld and McDonnell*, 2006] and its influence on overland flow are described in *Frei et al*. [2010].

**Table 1.** Surface and Subsurface Parameters Used in the Lehstenbach Catchment Model[a]

| | Parameter | Value |
|---|---|---|
| | *Surface* | |
| Forest | Manning's roughness $n$ | $1.9 \times 10^{-6}$ d/m$^{1/3}$ |
| | Rill storage | 0.5 m |
| Wetlands | Manning's roughness $n$ | $8.1 \times 10^{-5}$ d/m$^{1/3}$ |
| | Rill storage | 0.1, 0.5, and 1 m |
| Stream | Manning's roughness $n$ | $4.0 \times 10^{-7}$ d/m$^{1/3}$ |
| | Rill storage | 0.0 m |
| *Surface/Subsurface Coupling* | Coupling length | 0.1 m |
| | *Subsurface* | |
| Bottom, Middle, and Top Layer | Hydraulic conductivity $K_{sat}$ | 0.24 m/d |
| | Porosity | 0.4 |
| | van Genuchten $\alpha$ | 2.69 m$^{-1}$ |
| | van Genuchten $\beta$ | 1.45 |
| | Residual saturation $\theta_r$ | 0.1 |
| Wetland Layers (Bottom-Top) | Hydraulic conductivity $K_{sat}$ | 0.01, 0.02, 0.05, 0.13, 0.29, 0.68, 1.59, 3.69, 8.60, and 20.00 m/d |
| | Porosity | 0.5 |
| | van Genuchten $\alpha$ | 3.5 m$^{-1}$ |
| | van Genuchten $\beta$ | 1.7 |
| | Residual saturation $\theta_r$ | 0.1 |
| Clay Layer | Hydraulic conductivity $K_{sat}$ | 0.86 m/d |
| | Porosity | 0.45 |
| | van Genuchten $\alpha$ | 1.55 m$^{-1}$ |
| | van Genuchten $\beta$ | 1.26 |
| | Residual saturation $\theta_r$ | 0.1 |
| | *Evapotranspiration* | |
| Wetlands and Forest | Evaporation depth | 0.5 m |
| | Transpiration fitting parameter c1 | 0.2 |
| | Transpiration fitting parameter c2 | 0.5 |
| | Transpiration fitting parameter c3 | 1.0 |
| | Wilting point | 0.24 |
| | Oxic limit | 1.0 |
| | Anoxic limit | 1.0 |
| | Limiting saturation (minimum) | 0.24 |
| | Limiting saturation (maximum) | 0.4 |
| | Canopy storage parameter | $1 \times 10^{-6}$ m |
| | Initial interception storage | $1 \times 10^{-6}$ m |
| Wetlands | Root depth | 0.8 m |
| | Leaf area index | 3.0 |
| | Field capacity | 0.35 |
| Forest | Root depth | 3.0 m |
| | Leaf area index | 6.5 |
| | Field capacity | 0.34 |

[a]For a detailed description of all model parameters used in HGS, see *Therrien et al*. [2009].

### 3.2.2. Catchment Model Setup

[19] A digital elevation model (DEM) with a spatial resolution of 5 m × 5 m is used to represent the bowl-shaped topography of the catchment. Vertically, the model is discretized into two main geological units of variable thickness to represent the major soil types and subsurface geology of the Lehstenbach catchment. Within the wetland areas, the upper surface unit (1 m thick) represents the organic peat soils. This upper unit is represented in the grid by 10 sublayers of uniform vertical thickness equal to 0.1 m (see Table 1).

[20] For the 10 sublayers, the saturated hydraulic conductivity ($K_{sat}$) decays exponentially with depth to account for effects related to the transmissivity feedback mechanism, which has been described for peat forming wetlands [*Bishop et al*., 2004; *Jacks and Norrström*, 2004]. Values for $K_{sat}$ for the different sublayers ranged between 20 m/d for the uppermost layer (representing fresh and less compacted organic material) and $8.6 \times 10^{-3}$ m/d for the basal clay layer, which separates the wetlands from the deeper aquifer (Table 1). The values for $K_{sat}$ for the wetland areas are within the range reported by *Jacks and Norrström* [2004], who performed slug tests for similar wetlands located in the Luntoma catchment in Southwestern Sweden. The lower model unit (20–40 m thick) is represented in the grid by 10 sublayers and is used to represent the main regolith aquifer. Similar to the wetland model, parameters for the soil-water retention functions are applied uniformly to the upper wetland layers based on field measurements from similar wetlands in Alberta, Canada [*Price et al*., 2010]. Uniform parameters for the van Genuchten model as well as for $K_{sat}$ (0.24 m/d) of the main regolith aquifer are obtained from a previous calibration of the model to field observations of aquifer heads and stream discharge at the catchment outlet for the 2000–2001 hydrological year (1 November 2000 to 31 October 2001) [see *Werb*, 2009].

[21] Horizontally, the model uses a triangular mesh with variable node spacing (Figure 4). Nodal spacing in the mesh

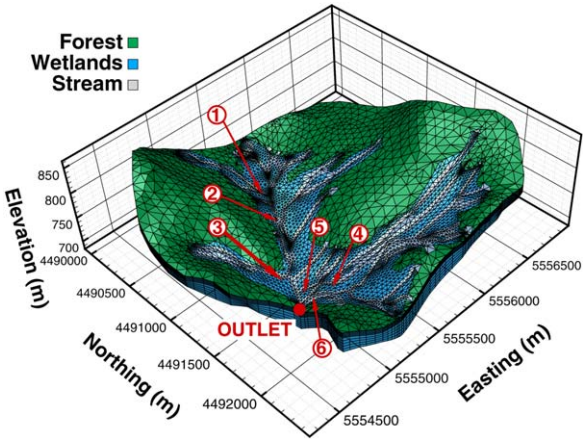


**Figure 4.** Model spatial discretization of the Lehstenbach catchment and distribution of the stream, wetland, and forest areas (the *z* axis is exaggerated by a factor of 5). Model observation points are at locations 1–6 and at the outlet.

varies between 10 m in the direct vicinity of the streams, 30 m within riparian wetlands, and 100 m for upslope areas. Within HGS, the locations of streams develop from flow between the surface and subsurface and tend to occur at topographical lows. However, the DEM used is too coarse to resolve differences in elevation between stream channels and the surrounding areas. Therefore, the elevations of surface nodes which coincide with stream locations are manually lowered by 1 m to correct for the smoothing of topography in the coarse DEM. For the subsurface flow domain, the bottom and lateral model boundaries are set to no flow to represent the contact with the low-permeability granitic bedrock and because it can be assumed that there is no exchange of groundwater with areas located outside of the Lehstenbach catchment. For the surface flow domain, a combination of variable rainfall, interception, and evapotranspiration is applied over the catchment. Interception and evapotranspiration [*Panday and Huyakorn*, 2004], within HGS, are simulated as mechanistic processes governed by plant and climatic conditions, as described by *Kristensen and Jensen* [1975] and *Wigmosta et al*. [1994]. At the edges of the surface flow domain, a critical depth boundary is used to simulate surface water outflow from the model. Manning's roughness coefficient for the forested upslope areas is assigned a constant value of $1.9 \times 10^{-6}$ d/m$^{1/3}$, representing areas of minor ground vegetation [*Shen and Julien*, 1993]. The friction slope for the wetlands is set to $8.1 \times 10^{-5}$ d/m$^{1/3}$, typical for high grass [*Shen and Julien*, 1993].

[22] Topography and land use for the Lehstenbach catchment are shown in Figure 4. The arrangement of mesh elements shown in Figure 4 is used to delineate the stream, wetlands, and forest areas. The detailed microtopography of the wetland model cannot be included explicitly at the catchment scale due to computational constraints. Instead, the rill storage concept is used [see *Therrien et al*., 2009], whereby a ponding depth is specified at surface nodes which must be reached before surface flow is induced. Spatially distributed rill storage height zones are used to represent the microtopographically induced threshold-type behavior of runoff generation from the wetlands. These storage zones mimic the depression-storage characteristics and the typical fill and spill mechanisms of the wetlands' microtopography. However, the behavior of the wetlands in the catchment-scale model (as opposed to the wetland model) is influenced additionally by variable groundwater heads at the upslope boundaries, which are driven largely by recharge originating from infiltration in the upslope forested areas. The simulation period is the hydrological year 2000 (1 November 2000 to 31 October 2001), although a focus is placed on the large July storm (13–21 July 2001) simulated in the wetland model. Note that because the whole year is simulated in the catchment model, day 0 in the wetland model is the same as day 200 in the catchment model. Evaluation of simulated stream discharge to the observed discharge for the 2001–2005 hydrologic years yields a Nash-Sutcliffe efficiency of 0.51, which is deemed reasonable for this study.

### 3.3. HMC Method

[23] The HMC method developed by *Partington et al*. [2011] allows separation of the streamflow hydrograph by the in-stream flow generation mechanisms (i.e., groundwater discharge to the stream, direct rainfall to the stream, and overland flow to the stream). The HMC method works by utilizing the spatiotemporal information of active in-stream flow generation mechanisms to obtain the contributing flow generation mechanisms. The HMC method treats each stream node in the surface domain of the model as a mixing-cell. The method utilizes the nodal fluid mass balance from the ISSHM at each model time step, to calculate the fraction of water in each cell that derives from different in-stream flow generation mechanisms. For example, if a cell has a water volume of 0 units at the start of the time step and 2 units at the end of the time step, and during that time step 1 unit of groundwater discharged into the cell and 1 unit of rainfall fell on the cell, then the fraction of groundwater discharge and direct rainfall in the cell would be 0.5. This becomes more complex if there is also outflow from the cell, because a mixing rule must be chosen for the mixing cells, which dictates how the fractions are calculated at the end of each time step. The HMC method uses the "modified mixing rule," which simulates a mixing regime between perfect mixing and piston flow [see *Campana and Simpson*, 1984].

[24] Each in-stream flow generation mechanism is assigned a unique fraction *f*. Over each time step of the model simulation, inflowing water into a cell from either the subsurface (e.g., groundwater discharge) or surface boundary conditions (e.g., rainfall) is classified by the corresponding unique fraction. The sum of all fractions in each cell, for an error-free fluid mass balance, is equal to 1. Inflow from adjacent cells is assigned the fractions from the upstream cell. *Partington et al*. [2011] derived an equation for the fraction *f* for each in-stream flow generation mechanism *k* at time *N* in cell *i* as:

$$f_{i(k)}^{N} = \left( \frac{V_i^{N-1}}{V_i^{N}} - \frac{\sum_{j=1}^{m} V_{ij} \Big|_{N-1}^{N}}{V_i^{N}} \right) f_{i(k)}^{N-1} + \frac{\sum_{j=1}^{n} V_{ji} \Big|_{N-1}^{N} f_{j(k)}^{N-1}}{V_i^{N}} \qquad (1)$$

[25] Where there are $n$ sources and $m$ sinks for cell $i$; ${f_{j(k)}}^{N-1}$ denotes fraction $k$ at time $N-1$ in the neighboring cell $j$, $V$ denotes the volume with the superscript denoting time state and subscript $i$ denoting the cell, $ij$ denoting volume into cell $j$ from cell $i$ over the time step from $N-1$ to $N$, and $ji$ denoting volume from neighbor $j$ into $i$.

[26] To achieve the aims of the current study, some limitations from previous implementations of the HMC method must be addressed. First, *Partington et al*. [2011, 2012] does not consider the contributing mechanisms for overland flow, as groundwater discharge adjacent to the stream was negligible. Second, *Partington et al*. [2011] notes that the HMC method was only numerically stable if the ratio of outflow to storage was less than 1, and the fluid mass balance convergence criterion was very small ($<10^{-10}$ m$^3$/s). These stability conditions require very low convergence criterion ($<10^{-10}$ m$^3$/s) for the solution of the fluid mass balance equation, and very small time steps ($<100$ s), thus increasing simulation time significantly. Use of the HMC method in this study expands on previous implementations by: (1) accounting for overland flow generation mechanisms in the HMC method, (2) modifying the HMC scheme to allow operation at subtime steps of the ISSHM flow solution time step, and (3) developing stability handling criteria for HMCs to prevent instabilities from occurring. Addressing these limitations enables the quantification of contributing in-stream and overland flow generation mechanisms for the more complex virtual experiment considered in this current study.

#### 3.3.1. Capturing In-Stream Overland Flow Generation Mechanisms

[27] Overland flow generation mechanisms are considered by using additional HMC fractions to those used in *Partington et al*. [2011, 2012]. All in-stream and overland flow generation mechanisms are delineated by surface node definition: e.g., "stream" or "overland." Surface nodes may also be defined as "other" nodes, which could be lakes, reservoirs, upstream inflow boundaries, or areas for which internal flow generation may not be of interest or are not known. In this study, forested areas are treated as "other" nodes. With respect to groundwater discharge and rainfall, flow generation at "other" nodes is not captured explicitly. Instead, any water flowing from "other" nodes to a stream or overland node is assigned an "other" fraction of 1 (i.e., $f_{other}=1$), i.e., without delineation of this water into components of groundwater discharge and rainfall. Unless water in the surface domain at the start of a simulation is assigned stream, overland or "other" fractions from a previous simulation, then it is not possible to know which flow generation processes were responsible for initial surface water. Therefore, an "initial" fraction is also included; initial conditions for existing surface water in each cell default to the "initial" fraction (i.e., $f_{initial}=1$, and all other fractions are set to zero) unless predefined otherwise.

#### 3.3.2. Subtimed HMC Algorithm to Ensure Stability

[28] The stability of equation (1) in the HMC method is dependent on the ratio of outflow to storage [*Partington et al*., 2011]. Stability requires that the volume of water leaving a cell over a given time step is less than the volume in storage. The volume leaving a cell is calculated using the fluid mass balance, accounting for small errors in the water balance (i.e., $\sum {f_{i(k)}}^N \neq 1$) within each cell (for outflow and storage). Absolute error ($\epsilon$) within cells is calculated as $\epsilon = |1 - \sum {f_{i(k)}}^N|$. The HMC ratio for each cell $i$ is defined as:

$$\text{HMC ratio}\,(i) = \frac{\sum_{j=1}^{m} V_{ij}\Big|_{N-1}^{N} f_{i(k)}^{N-1}}{V_i^{N-1}\sum_{\forall k} f_{i(k)}^{N-1}} \tag{2}$$

[29] Instability in the HMC method results when the cell ratio is greater than 1 in any HMC. For small HMCs, the storage volume may be quite small relative to the outflow. Maintaining the HMC ratio below 1 can necessitate very small time steps when the cell's storage is small relative to the flow. This is problematic for long-term transient simulations requiring large time steps in the flow solution. As part of the improved HMC method, a subtimed HMC method is implemented to prevent relatively small time steps of the HGS flow solution. This implementation removes the stability restriction (i.e., equation (2)) imposed by the HMC method on the maximum time step for the HGS flow solution. The subtimed HMC method is applied when the maximum HMC ratio at any of the cells is greater than 1. It works by subdividing the fluxes and storage changes within a time step. This subdivision between time steps $N-1$ and $N$, and calculation of fractions at each subtime step $n$ is done in the following way:

[30] 1. Calculate the number of subtime steps ($s$) required to ensure stability based on maximum HMC ratio:

$$s = [\max.\,\text{HMC ratio}\,] + 1 \tag{3}$$

where max. HMC ratio is the maximum HMC ratio.

[31] 2. Calculate the subtimed ratios ($t_{sub}$) for adjusting inflows, outflows, and storage changes at each $n$:

$${t_{sub}}^n = \left\{ \begin{array}{c} 1/(s-1); 1 \le n < s \\ 1 - {t_{sub}}^1 * (s-1); n = s \end{array} \right\} \tag{4}$$

[32] 3. Calculate the changes in storage for the cells over the whole time step:

$$dS_i = V_i^N - V_i^{N-1} \tag{5}$$

[33] 4. Calculate the subtimed HMC fractions, updating for all cells $i$ at each substep $n$ as follows:

$$f_{i(k)}^n = \left( \frac{V_i^{n-1}}{V_i^n} - \frac{\sum_{j=1}^{m} V_{ij}\Big|_{N-1}^{N} * {t_{sub}}^n}{V_i^n} \right) f_{i(k)}^{n-1} + \frac{\sum_{j=1}^{n} V_{ji}\Big|_{N-1}^{N} f_{j(k)}^{n-1} * {t_{sub}}^n}{V_i^n}, n = 1, ..., s \tag{6}$$

**subject to**

[34]

$$V_i^0 = V_i^{N-1} \text{ and } f_{a(k)}^0 = f_{a(k)}^{N-1}, \quad a = i,j \tag{7}$$

$$V_i^n = V_i^{N-1} + n * {t_{sub}}^n * dS_i \quad \text{for } 1 \le n < s \tag{8}$$

$$V_i^s = V_i^N \tag{9}$$

#### 3.3.3. Stability Constraints for Efficient Execution of the HMC Method

[35] The subtimed HMC scheme allows time steps in the flow solution to be as large as convergence criteria allow. However, a very large HMC ratio (>10,000), results in a large number of subtime steps. In terms of computational efficiency, a very large HMC ratio is not desirable, particularly for cells that only have very small volumes of water storage. In near dry cells, large HMC ratios will often arise at the onset of rainfall, groundwater discharge, or overland flow, as the outflow can be significantly larger than storage. The large HMC ratio problem tends to occur in simulating ephemeral reaches of streams whereby particular stream cells become dry. Similarly, this problem occurs in simulating overland flow whereby the overland cells are often dry (due to overland flow only normally occurring in rainfall events). In these cases of a large HMC ratio, particular cells can become numerically unstable due to propagation of errors from the fluid mass balance. Fortunately, this occurs at cells that are of little interest in a physical sense (i.e., where active processes take place but with relatively insignificant volumes of water).

[36] To address these problems and ensure stability and computational efficiency, criteria are added to the method and used to determine if each cell should be evaluated. If any of these criteria are met, then the cell being evaluated is reset, which means that all fractions $f$ in the reset cell are set equal to zero, and that the cell is assigned the reset fraction ($f_{\text{reset}} = 1$). The criteria (a–e below) for a reset cell are checked at each time step, allowing it to become active if the reset criteria are no longer met. The reset fraction allows the tracking of the fraction of water for which the flow generation is unknown (due to the cell being reset), which quantifies the effect of the reset fraction. Tracking of the reset fraction highlights through inspection of calculated HMC fractions if this unknown flow generation is significant. If the reset fraction of flow in the streamflow hydrograph is high (>1%) then each criterion can be modified to bring this to a satisfactory level (<1%).The reset criteria are as follows:

[37] (a) *Minimum volume*. Cells with relatively small water storages are reset unless surface flow is greater than zero ($10^{-10}$ in this study).

[38] (b) *Ponding only*. Cells with no surface flow are reset if the inflow or outflow is greater than the volume of ponded water.

[39] (c) *Maximum HMC ratio*. Cells with a large HMC ratio (equation (2)) are reset ($10^4$ in this study).

[40] (d) *Relative volume error too high*. Cells in which the ratio of the "absolute volume error" to storage is large are reset, where the absolute volume error denotes the absolute value of the error in the volumetric cell balance (2.5 in this study).

[41] (e) *Error in HMC excessive*. Cells with a large absolute error ($\epsilon$) are reset after updating the fractions in the cell at each time step or subtime step (0.5 in this study).

## 4. Flow Generation Analyses Conducted Using the HMC Method

[42] The in-stream and overland flow generation mechanisms analyzed for the case study (see Figure 2) are: (1) groundwater discharge to the stream channel (GW-CH), (2) direct rainfall to the stream channel (RF-CH) and overland flow to the stream channel. The overland flow generation mechanisms analyzed are: (3) groundwater discharge to wetland surface areas (GW-WL), (4) direct rainfall on wetlands surface (RF-WL), and (5) overland flow from forested areas (Forest).

**Table 2.** Considered Flow Generation Mechanisms, HMC Unique Fractions, and HMC Fraction Types

| Flow Generation Mechanism | Unique Fraction | Fraction Type |
|---|---|---|
| Groundwater discharge to the stream channel | GW-CH | In-stream |
| Direct rainfall to the stream channel | RF-CH | In-stream |
| Groundwater discharge to the wetlands | GW-WL | Overland |
| Direct rainfall to the wetlands | RF-WL | Overland |
| Surface flow from the forest area | Forest | Other |
| Unknown | Initial | Initial |
| | Reset | Stability |

[43] The unique fractions $f$ used in this HMC analysis are: (1) GW-CH, (2) RF-CH, (3) GW-WL, (4) RF-WL, (5) Forest, and also (6) initial water (Initial) and (7) reset water (Reset). In-stream and overland flow generation mechanisms are determined based on surface cell type: i.e., stream, wetland, or forest cells. Each analysis outlined below corresponds directly to aims 1–3. To aid the reader through the following sections, Table 2 summarizes the flow generation mechanisms analyzed, and the corresponding unique HMC fractions and fraction types.

### 4.1. Separating Flow Hydrographs by In-Stream and Overland Flow Generation Mechanisms

[44] The main output from the HMC method is the values of the unique fractions $f$ at each cell, which are used to separate the flow hydrographs by multiplying the total flow at each time step by each of the unique fractions at the corresponding time step. Each flow hydrograph at the outlet and selected model observation points (see Figures 3 and 4) is made up of a collection of cells. At each cell, the surface outflow is separated by the unique fractions into the corresponding flow generation mechanisms, and then these are summed for each collection of cells.

### 4.2. Analyzing Spatiotemporal Variability of In-Stream and Overland Flow Generation

[45] Spatial and temporal variability of in-stream and overland flow in both models is demonstrated in three ways. First, visualization of the HMC fractions across the model surface domain is shown in each model at different points in time. Second, flow hydrographs are shown at select observation points within each of the models. Last, the different flow generation mechanisms driving total flow at each of the locations are summarized. The summarizing of the flow components is achieved by integrating over the flow curves for each of the flow generation mechanisms, at each selected observation point.

### 4.3. Analyzing Active and Contributing Processes

[46] The analysis of active and contributing processes is carried out over the entire year-long simulation for the catchment-scale model. In particular, the components analyzed are GW-CH, RF-CH, and wetlands surface discharge

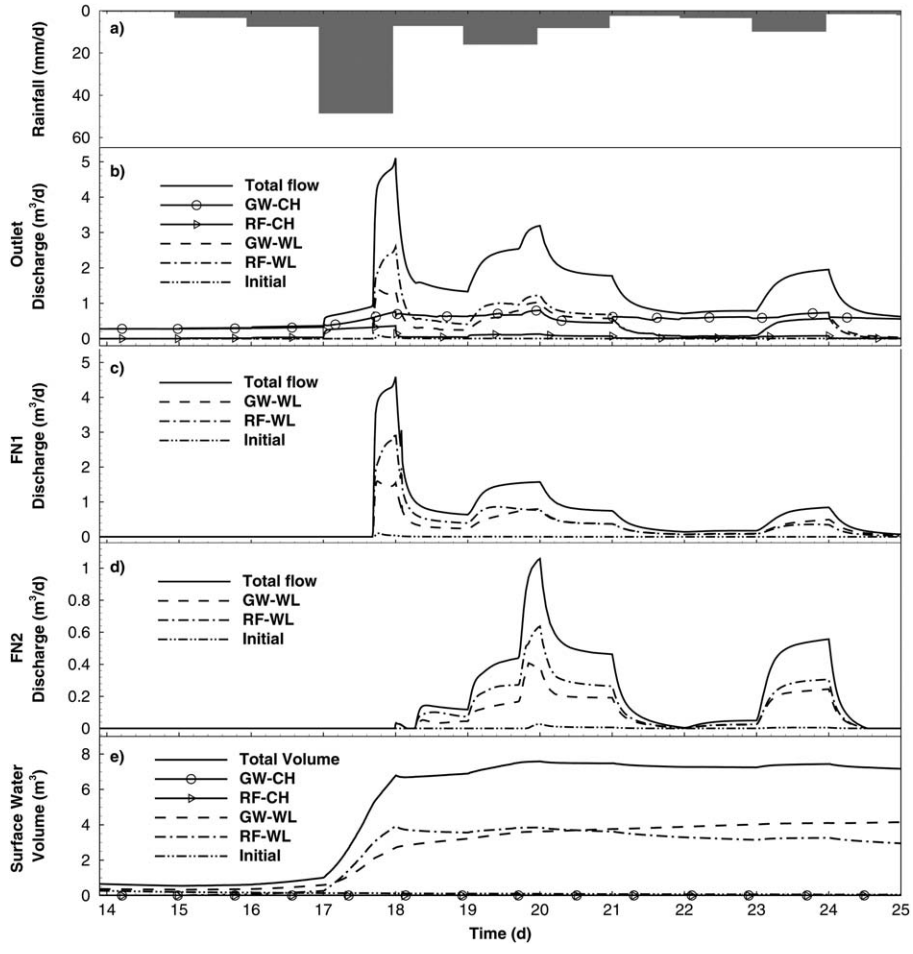


**Figure 5.** Hyetograph, simulated outlet hydrograph, simulated FN1 hydrograph, simulated FN2 hydrograph, and simulated surface water storage graph for the wetland model during a large storm event. GW-CH and RF-CH are direct groundwater discharge and rainfall to the channel. GW-WL and RF-WL represent groundwater discharge and rainfall to the surface of the wetland area, respectively. Initial represents the initial water in the surface domain at the beginning of the simulation. The reset fraction of flow was negligible ($<1 \times 10^{-12}$%) and hence is not shown.

to the stream channel (WL-CH = GW-WL + RF-WL). Runoff from the forested areas to the stream channel is also considered (Forest-CH). The active flow generation processes are determined by summing the inflowing fluxes to the surface domain (GW-CH, RF-CH, WL-CH, and Forest-CH) at each time step, and the contributing processes (taken at the outlet) are determined from the HMC analysis. A long-term ratio of contributing to active flow generation mechanisms is calculated to quantify the cumulative difference between these two.

## 5. Results and Discussion

### 5.1. Wetland Model

#### 5.1.1. In-Stream and Overland Flow Generation Mechanisms Driving Flow

[47] The applied rainfall and the resultant outflow and corresponding flow generation components are shown in Figures 5a and 5b. From the time rainfall starts, streamflow increases slightly until day 17, at which point the rainfall rate increases significantly. The rain falling directly on the channel contributes to runoff immediately. The infiltration across the overland area increases the subsurface head, which in turn increases the groundwater discharge to the channel. The rapid response of rainfall directly on the channel (RF-CH) is clearly seen to follow the pattern of the rainfall input. During the highest rainfall period, over day 17, the groundwater discharge to the channel rises to an apparent quasi-steady state. In the 4 days that follow, the GW-CH component only changes slightly in relation to the total streamflow. All major changes in streamflow between days 17 and 22 are attributed to changes in overland flow to the stream. It can be seen in Figure 5c that at approximately 17.6 days, overland flow from FN1 reaches the channel and causes a rapid increase in streamflow. Figure 5d shows that almost half a day after FN1 starts discharging to the channel, at approximately day 18, FN2 starts contributing to streamflow. Whilst a greater proportion of rainfall to the wetland surface area (RF-WL) is evident, there is also a large component of groundwater that discharged to the wetland surface (GW-WL). This large component of GW-WL in the outflow hydrograph appears not only to be an

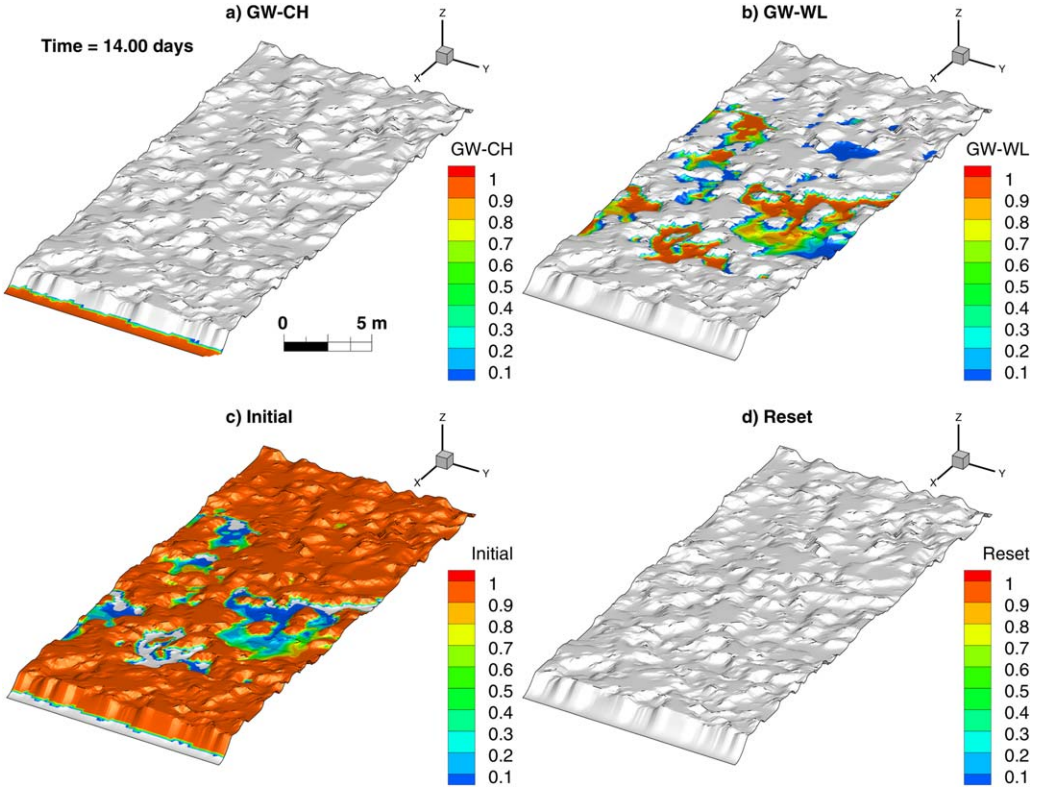


**Figure 6.** Wetland HMC fractions at day 14 (prestorm event). The in-stream and overland flow generating mechanisms shown are: (a) groundwater discharge to the channel (GW-CH), (b) groundwater discharge to the wetland surface (GW-WL). The (c) initial and (d) reset fractions are shown. A GW-WL fraction of 0.5 denotes that 50% of the water at that cell was generated from groundwater discharging to the wetland surface.

increase in this overland flow generation mechanism at this particular time but also a result of the mobilization of the ponded water generated from GW-WL. The total surface water storage across the model and also the flow generation mechanisms that created the storage are shown in Figure 5e. The ponding of water in the hollows makes up almost 100% of the surface storage (with the GW-CH and RF-CH water being relatively insignificant). There is only a relatively small variation in the total storage after day 18. A small component of initial water is contributing to streamflow at the outlet at day 18. The initial water is mobilized after the hollows fill and then spill toward the stream. This shows a slow rate of turnover (>18 d) of ponded surface water due to the time taken for the hollows to "fill and spill," i.e., prior to the activation of the flow networks.

### 5.1.2. Spatiotemporal Variability of In-Stream and Overland Flow Generation

[48] Two snapshots of in-stream and overland flow generation are shown for the wetland model, just before the rainfall event at the start of day14 (Figure 6), and 6 days into the storm event at day 20 (Figure 7). The distributions of (1) GW-WL water in the hollows and (2) GW-CH water are shown in Figures 6 and 7. After 14 days, the rainfall event begins and therefore there is no RF-CH or RF-WL fraction of surface water (not shown in Figure 6). The reason that the fraction of GW-WL water is not equal to 1 across the hummocks and hollows is because of the persistence of initial water, of which a small volume resides on the surface.

[49] The development of overland flow in the wetlands is well established at day 20. An increase in the GW-WL component of streamflow is explained by the increased subsurface heads leading to a larger seepage face along the bank. Close examination of the two flow networks (FN1 and FN2) highlights variations in the overland flow generation across the wetland. The overland flow network FN1 has a slightly higher component of groundwater discharge, whereas the flow network FN2 has a slightly higher component of rainfall, with clear spatial variation in each. The flow network FN2 has a higher rainfall-driven component because of the larger surface area of the stored water, which receives more rainfall. The reset of cells at the top of the hummocks and the upper part of the stream bank is due to the fact that these cells have no surface flow to other cells and also the inflow from rainfall at these cells is much greater than the ponded water volume.

[50] Figure 8 shows a summary of the percentage of total volume of water derived from different in-stream and overland flow generation mechanisms. This summary is provided at the outlet and for each of the flow networks (FN1 and FN2). All volumes are determined by integrating over the flow hydrographs in Figures 5b–5d. The contributions toward total flow from the two overland flow networks are calculated to be 34% and 10% for FN1 and FN2, respectively, making a total overland flow contribution of 44% over the simulation period. The components of initial water and reset water are insignificant (<1%). The volume

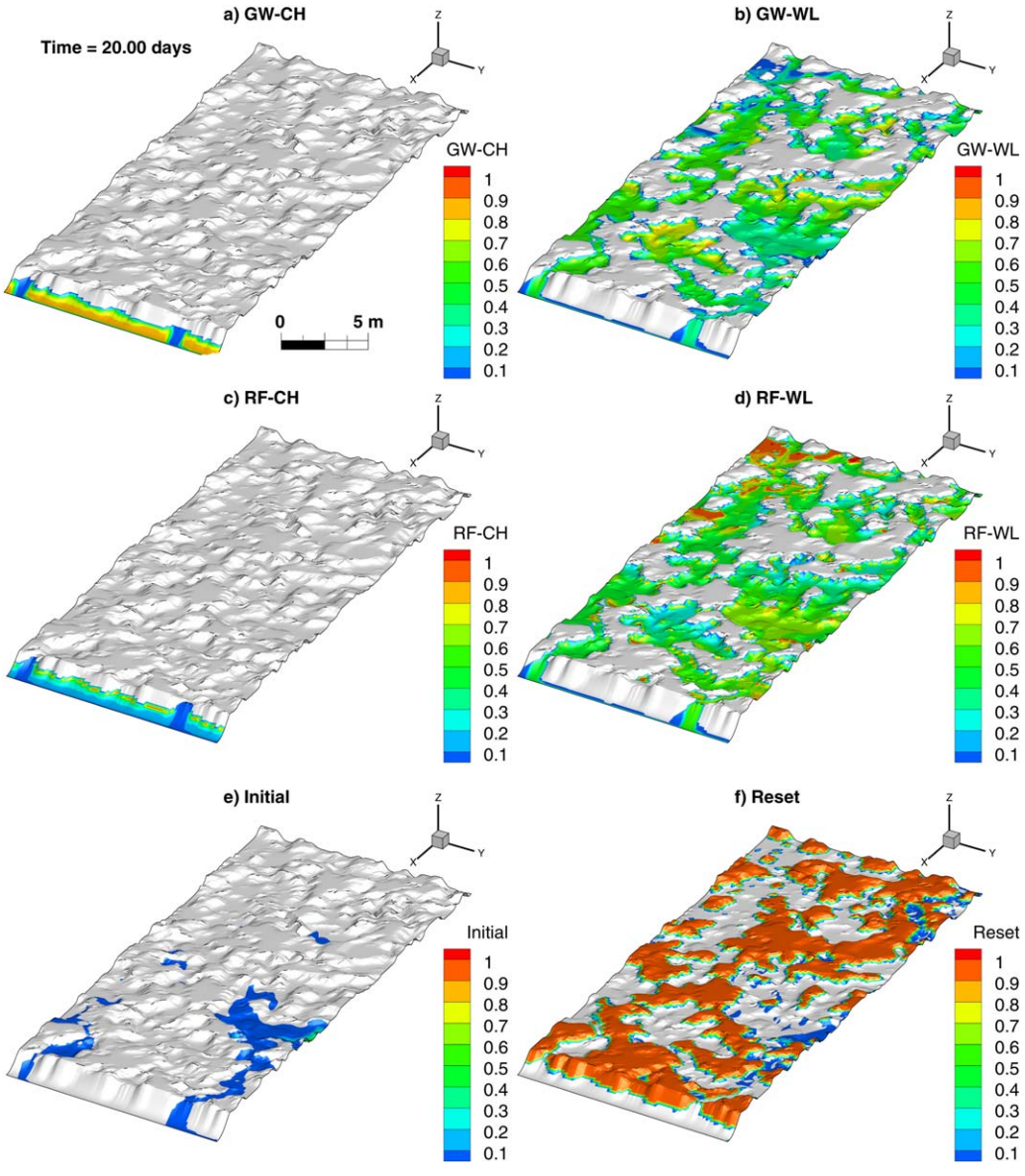


**Figure 7.** Wetland HMC fractions at day 20 (during the storm event). In-stream and overland flow generating mechanisms shown are: (a) groundwater discharge to the channel, (b) groundwater discharge to the wetland surface, (c) rainfall to the channel, (d) rainfall to the wetland. (e) The remaining initial water and (f) the reset fraction for reset cells are also shown.

attributed to cumulative error is extremely small at the outlet ($4 \times 10^{-16}$%).

[51] To summarize, HMC analysis of the wetland model demonstrates clear spatial variability in overland flow generation, as depicted in Figures 6 and 7. This variability is clear in the discharge hydrographs of the two flow networks (Figure 5), highlighting a complex relationship between rainfall input and runoff from the wetlands into the stream. However, despite this spatial variability, the flow networks have similar compositions of overland flow generation components at the point of discharge into the stream, with both FN1 and FN2 being dominated by RF-WL flow generation (Figure 8). The HMC analysis shows that the RF-WL component of flow is larger by about 5% over the GW-WL component in driving the overland flow contribution at the outlet (Figure 8). As evidenced in the Figure 5 discharge hydrographs, the storage across the overland area shows that the relationship between overland storage and overland flow contributions to streamflow at the outlet is nonlinear. As noted in *Frei et al*. [2010], this nonlinear relationship is caused by the complex nature of the "fill and spill" mechanism. As expected, the direct RF-CH component of in-stream flow generation followed the rainfall input. This is because there are no significant time lags or losses along the stream and to the subsurface. Similarly, the response to rainfall of groundwater discharge to the channel (GW-CH) is also as expected, although it has a slower response than the RF-CH component.

### 5.2. Catchment Model

[52] Three snapshots from the model simulation for the large storm in July 2001 are examined for surface water

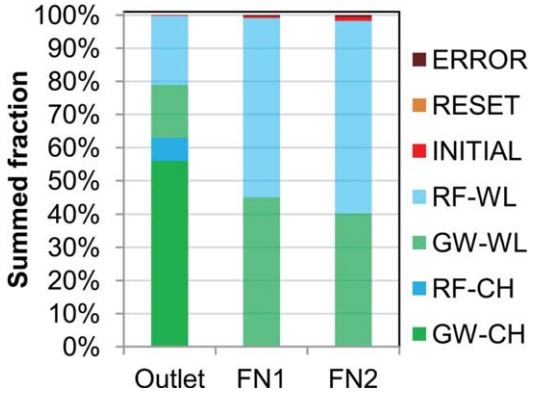


**Figure 8.** Comparison of different streamflow generation mechanism contributions at the outlet, FN1 and FN2. The initial and reset fractions and the cumulative error in the cells were insignificant, as can be seen at the top of the stacked columns.

distribution and surface-subsurface exchanges. These snapshots are taken just prior to the storm (day 216), at the peak of the storm (day 218), and 2 days after the peak (day 220). Figure 9 shows standard HGS outputs of surface saturation, exchange flux and depth distribution across the catchment at each of these times. Figure 9a shows that saturation at the surface boundary increases across the catchment as the storm event progresses. The exchange flux (Figure 9b) across the catchment shows where water is exfiltrating from the subsurface to the surface (positive values) and where water is infiltrating into the subsurface from the surface (negative numbers). Prior to the storm event, there is no exchange across the forested areas, water is being lost from the wetlands to the subsurface, and groundwater is discharging to the stream. At the peak of the storm, the infiltration rate peaks in the forested areas, but the infiltration from the wetlands decreases. The area of groundwater discharging to the stream is slightly increased, but not significantly. At the cessation of the storm event, the infiltration rate is varied across the forested area. In Figure 9b, at day 220, about two thirds of the reach on the right arm of the stream is losing (highlighted by a red ellipse).

[53] The surface water depth distribution (Figure 9c) across the catchment highlights the wetland areas, where most surface ponding occurs. Excluding the stream, these wetland areas lie at the lowest elevation in the catchment. It is these ponded wetlands that provide the overland runoff during the storm event. There is discharge of groundwater at the upper part of the right arm of the stream, however, this water is returned to the subsurface across the losing stretch of this reach of the stream (highlighted in Figure 9b).

#### 5.2.1. In-Stream and Overland Flow Generation Mechanisms Driving Flow

[54] The separated streamflow hydrograph at the outlet is shown in Figure 10. In Figure 10b, the GW-CH component of streamflow is seen to respond immediately to rainfall events with no clear lag, possibly due to propagation of a pressure wave. As rainfall ponds on the hydraulically connected wetlands, this in turn increases the head in the underlying aquifers. The GW-CH component of streamflow is seen to make up ~97% of the flow in dry periods—the GW-WL component of streamflow contributes a very small amount to streamflow during dry periods (~3%). The RF-WL and GW-WL components of the outlet hydrograph (Figure 10b) show that the wetlands only provide a significant component to streamflow during the larger storm events (e.g., at the storm peak, day 218). After the large storm event from day 221, the streamflow is supported mainly by GW-CH discharge to the stream. Overland flow from the forested areas had a negligible contribution to overland flow in the wetlands and hence also to total streamflow (<0.2%), and for this reason is not shown in the hydrographs.

[55] The total surface water storage across the Lehstenbach catchment and the storage of water from different flow generation mechanisms, i.e., the mechanism by which the water came into storage are depicted in Figure 10c. This figure shows that much of the storage in the surface is ponded water in the forested areas. The second largest component of storage is rainfall stored in the wetlands. Notably, the GW-CH and RF-CH generated surface storages are relatively insignificant with respect to total storage, yet provide the largest contribution to streamflow. The surface water volumes of initial, reset, and cumulative error are relatively insignificant (i.e., appear as horizontal lines along $y = 0$ in the graphs) to the flow generation mechanisms and are therefore not shown.

#### 5.2.2. Spatiotemporal Variability of In-Stream and Overland Flow Generation

[56] The in-stream and overland flow generation calculated by the HMC method (at the same snapshot times as in Figure 9) for the large July storm are shown in Figure 11. Prior to the storm, at day 216, the GW-CH component of streamflow over the entire stream is high and dominating. At this time, there are small patches of RF-CH generated stream water in places where little to no groundwater is discharging and where there is no upstream flow passing through. A portion of the wetland areas prior to the storm show GW-WL generated surface storage, a small portion of which is feeding into the stream, which is more clearly apparent in the hydrograph of Figure 10. The speckled RF-WL water existing prior to the storm highlights areas where some ponding from rainfall has occurred that is yet to either runoff, infiltrate, or evaporate. The source of this rain is attributed to smaller recent rainfall events (not shown). The bottom row of Figure 11 shows the amount of reset (or unknown) fraction across the catchment during the storm. Areas where the reset fraction is high correspond to areas where either no surface flow is occurring or ponding is insignificant (as defined in section 3.3.3). This highlights areas where ponding processes take place, but in such small quantities that they are not of interest, particularly in relation to the streamflow hydrograph. As noted in section 3.3.3, any reset cell is still tracked, which means that any surface flow out of a reset cell is also tracked so that the influence of these cells is accounted for.

[57] At the peak of the large storm, at day 218, the fraction of GW-CH generation becomes diminished across the stream as rainfall generation mechanisms become dominant. The reduction of the fraction of GW-CH generation is

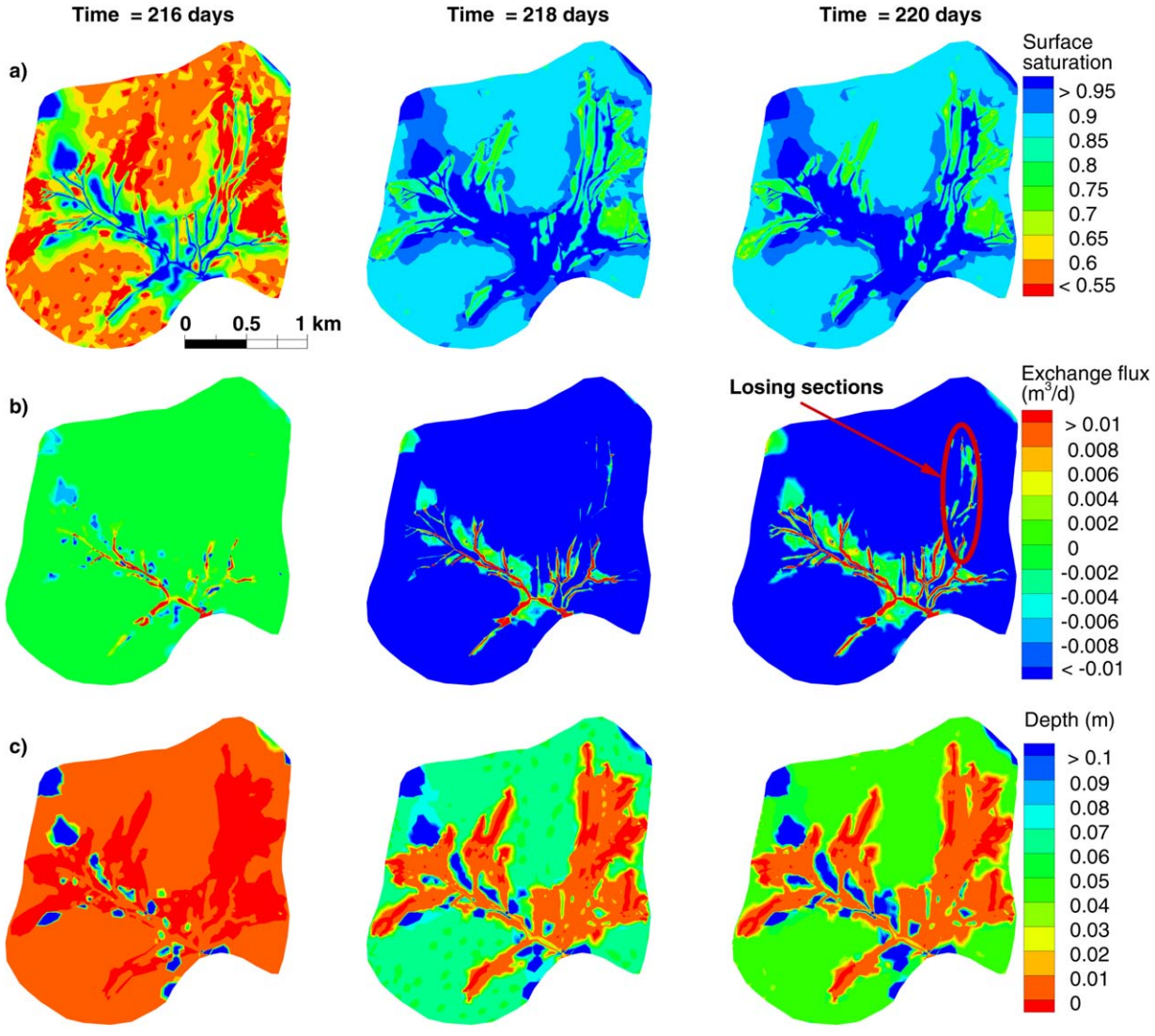


**Figure 9.** (a) Simulated surface saturation, (b) exchange flux, and (c) surface water depth, prior to the storm, at the storm peak and 2 days after the storm peak. A losing section on the right arm of the stream is highlighted in the third frame of Figure 9b. Positive values of exchange flux indicate groundwater discharge to the surface and negative values indicate infiltration of surface water to the subsurface.

matched by an increase in fractions of RF-CH, GW-WL, and RF-WL generation. At day 218, an increase in the active part of the stream on the right arm (including upstream of the losing section) is shown in the RF-CH generation. The GW-WL generation on the wetlands at the peak of the storm is reduced. However, it is worth noting that the GW-WL water appears in the same area as where water has ponded, shown in the depth distribution in Figure 9. As described in the stability criteria section (section 3.3.3), surface nodes containing less than $10^{-10}$ $m^3$ of water are excluded from analysis and are reset, which causes the "speckled" effect that is seen adjacent to the upper reaches of the stream. This effect is attributed partly to the spatial variations in rill storage height across the wetlands. The small water storage at some wetland nodes relates to those wetland nodes not being saturated and water infiltrating quickly due to the high hydraulic conductivity near the surface.

[58] After the peak of the storm event, at day 220, the GW-CH generation component starts to increase. This increase is most apparent in the lower reaches of the stream where the RF-CH generated streamflow has been mostly flushed from the stream. The RF-CH component is still strong in small isolated areas in upstream parts of the stream that are not flowing, and instead, are ponding. The wetlands receive more groundwater discharge after the storm, which is reflected in the extent of GW-WL generation across the catchment.

[59] Analysis of the entire 2001 hydrological year allowed comparison of the longer term flow generation across the catchment to the July large storm event. Figure 12 shows box plots of the percent contribution of each of the flow generation mechanisms across the seven model observation points depicted in Figure 4. The left plot shows the spread for the entire hydrological year and the right shows the spread for the large July storm (between days 17

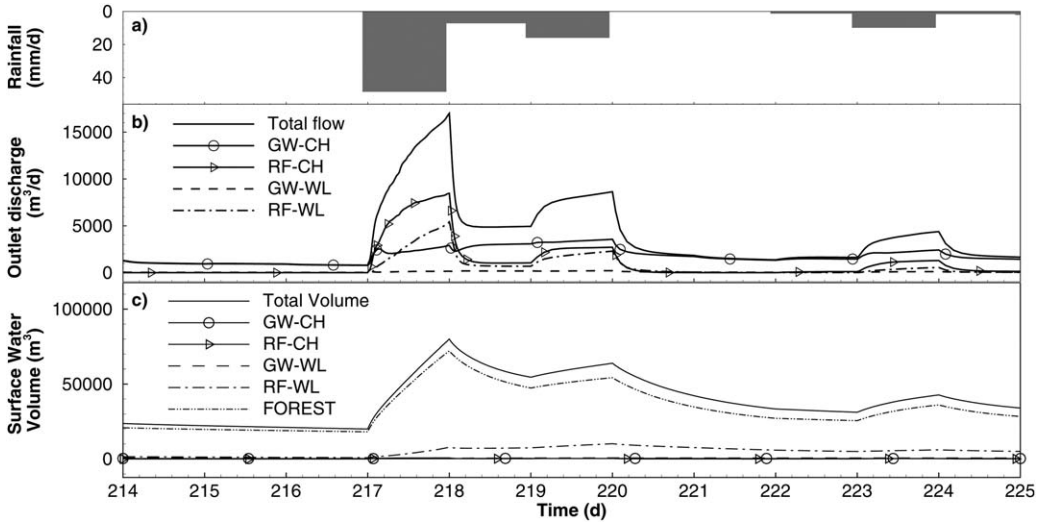


**Figure 10.** (a) Hyetograph, (b) separated simulated discharge hydrographs at the outlet, as well as (c) the HMC fractions in surface-storage across the catchment. Note that simulated overland flow from the forest was negligible (<0.2%) in contributing to streamflow and so is not shown in Figure 10b.

and 20). The volume of water that passed through the outlet and locations 1–6 is determined by integrating over the streamflow hydrographs for each component of flow and dividing by the total volume of streamflow that passed through. Not shown are the fractions of "forest" (maximum 0.3%), initial (maximum 0.05%), and reset (maximum 0.41%) and the cumulative error resulting from imperfect nodal fluid mass balances over the simulation (maximum −0.9%). These components are relatively insignificant in comparison to the four main flow generation mechanisms. This volumetric analysis indicates that the mechanisms for flow generation did not differ significantly across the Lehstenbach catchment, although greater variation can be seen across the focused period of the large July storm compared to the entire year. However, it is worth noting that the "outliers" in the "event" plot correspond to observation point 1, which contributes less than 1% of the flow over this event.

[60] Comparison of the distribution of individual flow generation processes across the entire hydrological year showed surprising uniformity across the catchment. The similarities in flow generation processes over the year-long time scale at the seven model observation locations are possibly due to the uniformly applied rainfall events and the simplified representation of the microtopography across the wetlands. The distributions for the event scale show a larger spread across the seven model observation locations, which was also evident in the individual hydrographs. This difference in the drivers of streamflow across these observation points is possibly due to timing of the activation of WL-CH flow across different areas of wetlands, and the differences in head gradient at the stream interface driving GW-CH flow.

[61] The catchment model shows a combination of simple processes varying in space and time, which leads to a complex culmination of in-stream and overland flow generation processes at the outlet. Rain falling in the forested areas mainly infiltrated and then recharged the underlying unconfined aquifer, which in turn fed the adjacent downslope riparian wetlands and stream. Because of the "rill storage" within the wetland areas, there is an aggregated "fill and spill" mechanism that is averaged over the wetland areas. The rill storage provided a threshold to rainfall inducing runoff from the wetland areas. The GW-CH response to rainfall mimicked a dampened rainfall input. This GW-CH component appeared more sensitive than the GW-WL component, which contributed very little to streamflow. The sensitivity of the GW-CH component is caused by the heads in the riparian wetlands controlling groundwater flow. As the wetlands and underlying unconfined aquifer are connected, increases in water levels in the wetlands from rainfall increases subsurface heads and hence increases the discharge of groundwater to the stream channel (i.e., GW-CH generation mechanism). Conversely, the slower, almost filtered response from the GW-WL generation mechanism is caused by: (1) the time delay in percolation recharging the unconfined aquifer from the forested areas; then (2) the slow flow of groundwater through the unconfined aquifers into the wetlands; then (3) the mobilization of ponded water in the wetlands into the stream once the wetlands overtop into the stream.

#### 5.2.3. Active Versus Contributing Flow Generation Mechanisms

[62] A comparison of the active and contributing flow generation processes for GW-CH, RF-CH, and WL-CH is shown in Figure 13. In Figure 13a, the active component of GW-CH flow is clearly seen to be higher than the contributing processes which predominantly result from losing areas along the stream. It should be noted that the time lags in the stream also lead to a difference between the active and contributing components, although these are small in this catchment and hence do not play an obvious role. Similarly, in Figures 13b and 13c, a much larger flux is evident of active RF-CH and WL-CH flow as opposed to the contributing portion at the outlet. This figure highlights the transient difference between the active and contributing processes in this catchment.

[63] The long-term ratio of contributing to active flow generation processes for WL-CH (0.78), RF-CH (0.34), and

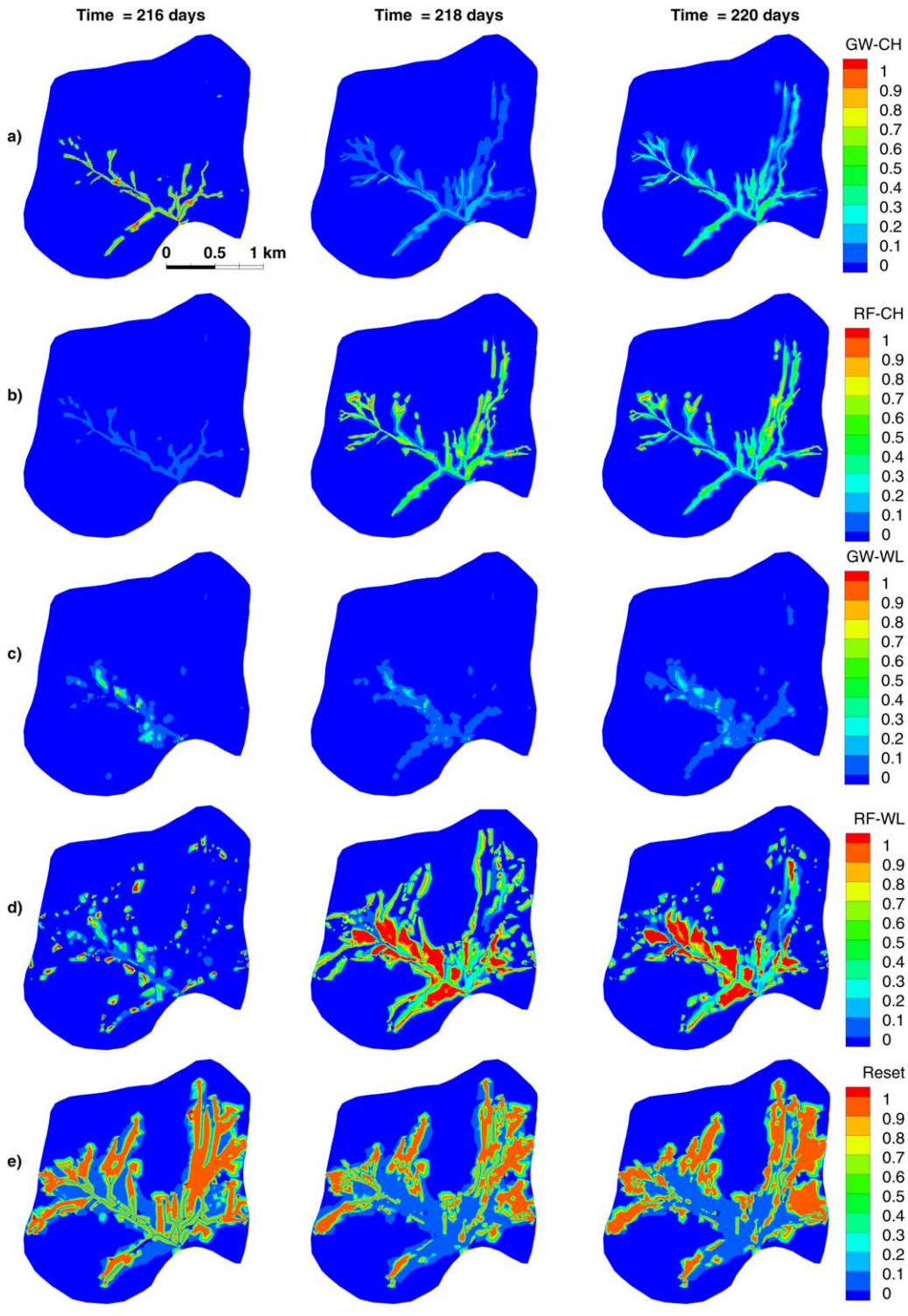


**Figure 11.** HMC calculated in-stream and overland flow generation for the Lehstenbach catchment—before peak (day 216), at peak (day 218), and after the peak (day 220). The flow generation components are: (a) groundwater discharge to the channel (GW-CH), (b) rainfall to the channel (RF-CH), (c) groundwater discharge to the wetland's surfaces (GW-WL), and (d) rainfall to the wetlands (RF-WL). The initial fractions are not shown as all initial water has been flushed from the catchment. (e) The reset fractions are shown.

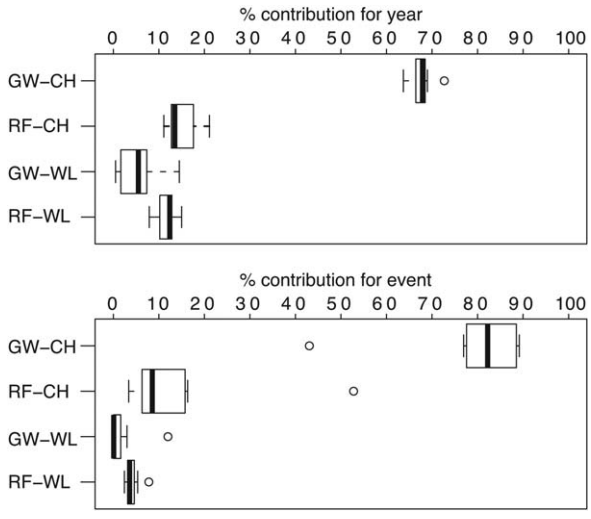


**Figure 12.** Box plots showing the spread of the average in-stream and overland flow generation mechanism contributions for the entire year and during the large storm event, across the seven different model observation points. The thick black line represents the median; the box covers the inter quartile range (IQR) bounded by the lower and upper quartiles; the whiskers extend to the lowest and highest data point within the fences (where the fences are 1.5 × IQR above and below the upper and lower quartiles, respectively); the circles represent data above and below the upper and lower fences, respectively.

GW-CH (0.25) highlights the significant differences between active flow generation processes across the catchment and contributing flow generation processes driving outflow. Furthermore, the cumulative lines show how this dichotomy develops through time. This supports the need to differentiate between these active and contributing processes in interpreting streamflow hydrographs, and therefore, the need to separate the streamflow hydrograph properly.

### 5.3. Comparison of Wetland and Catchment Models

[64] At the outlet of both models, GW-CH streamflow generation was fairly consistent across storms with only minor changes relative to the total streamflow hydrograph. The GW-CH component was seen to respond immediately to rainfall with no obvious lags in both models. Large changes in streamflow at the outlets for both models can be attributed to the overtopping of rills within the riparian wetlands driven by both RF-WL and GW-WL mechanisms. However, in the catchment model, the RF-CH component contributes significantly to total streamflow during the large storm event, which is attributable to the coarse model discretization of the stream network. This discretization does not capture the narrow nature of the actual channels, so that the channels in the model are wider than they are in reality. The surface area of the stream in the model captures additional rainfall that would not usually be attributed to the RF-CH flow generation mechanism within the catchment. Overland flow from the wetlands in both models is dominated by RF-WL flow generation. The GW-WL component is almost as large as the RF-WL component in the wetland

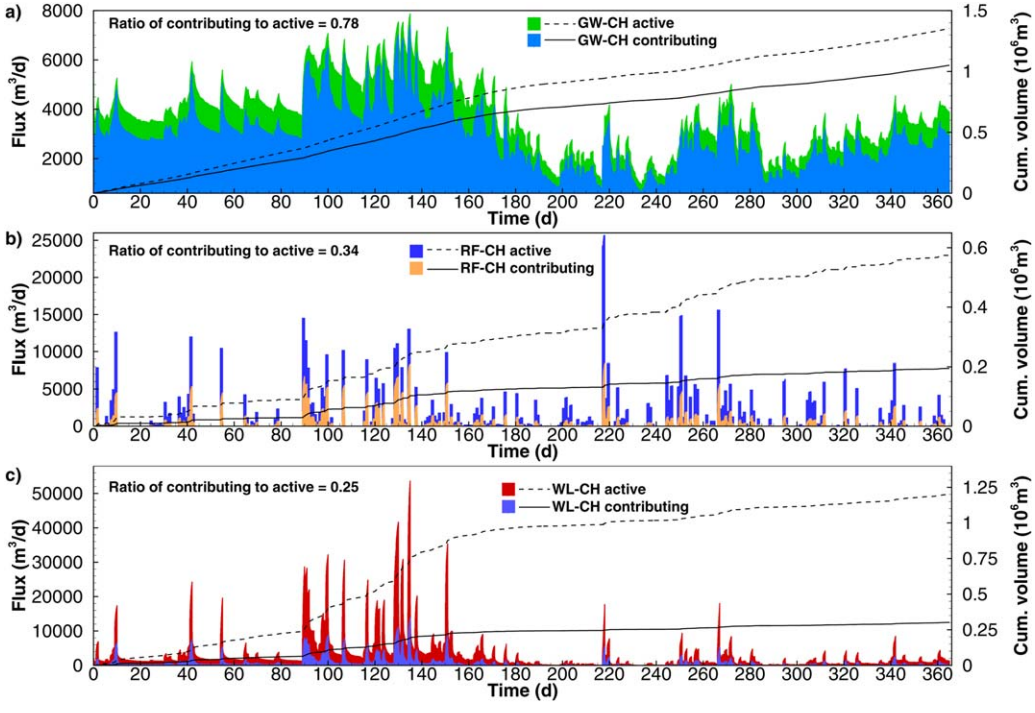


**Figure 13.** Comparison of active and contributing processes with respect to (a) GW-CH, (b) RF-CH, and (c) WL-CH (where WL-CH = RF-WL + GW-WL). Note that the contributing component is superimposed on top of the active component in each of these graphs, i.e., they are not stacked. The long-term ratio of contributing to active processes is also noted in each of the plots, which highlights the average difference between the two. The dashed and dotted lines on each plot represent, respectively, the cumulative active and contributing components.

model; however, the GW-WL component is almost negligible at the outlet of the catchment model. The difference in the GW-WL component between the two models can be attributed to the discretization of the wetlands. In the catchment model, the threshold behavior to overland flow is captured, which is evident in the wetland model, but the catchment-scale model does not capture the enhanced surface-subsurface mixing of the wetlands model, which results in a lot of the RF-WL water infiltrating and then discharging as GW-WL.

### 5.4. Limitations of Wetland and Catchment Models

[65] A number of assumptions were made within this modeling that limited the representation of reality, as well as any generalizations that can come from it. The main limitation of the wetland model is that it does not replicate a particular Lehstenbach wetland, hence there are no observed data to compare with, meaning the model can only be used for virtual experimentation.

[66] For the catchment-scale model, only outflow time series were available for calibration. As this was the only data used in evaluation of the model, there are likely to be multiple parameter sets that could yield the same Nash-Sutcliffe efficiency, i.e., equifinality. Alternative parameter sets with equivalent model fits could potentially lead to significant differences in the spatiotemporal distribution of flow generation processes and hence influence the dynamics of contributing processes at the catchment outlet. The resulting nonuniqueness of processes elicited with the HMC method might not be representative of the actual processes occurring in the Lehstenbach catchment. This limitation could be addressed (at least in part) by using additional hydrometric data in model calibrations to further constrain the problem.

[67] HMC analysis shows that the response of the wetlands in the catchment-scale model seems to be consistent with the understanding of wetland runoff processes and the catchment behavior in general; however, the effect of the mesh discretization of the stream and wetlands in the catchment model mesh on the GW-CH response and WL-CH response still requires quantification. Refining the coarse mesh would allow for better representation of the enhanced surface-subsurface mixing, as exhibited in the wetlands-scale model, which is important in consideration of biogeochemical processes [*Frei et al*., 2012].

[68] The subsurface response is affected by the subsurface boundary conditions, and no flow boundaries in the subsurface prevent groundwater from flowing out through the subsurface, which leads to increased groundwater exfiltration near the outlet. Although this is generally consistent with the understanding of subsurface flows in the catchment based on previous studies [*Hauck*, 1999; *Lischeid et al*., 2002], a more thorough assessment of the effects of the subsurface boundary conditions on catchment outflow would be helpful to further refine our understanding of the system.

[69] Model simulations would likely have been influenced by: (1) simplification of heterogeneity within soil types, (2) exclusion of preferential subsurface flow, and (3) spatiotemporal resolution of rainfall and evapotranspiration inputs (spatially uniform rather than distributed, daily rather than hourly rainfall and ET). It is expected that additional heterogeneity (e.g., within each soil layer) would lead to more complex stream-aquifer exchange patterns, although it is not expected that this would significantly alter the catchment response. Inclusion of shallow macropores in the forested areas of the catchment would allow rapid infiltration to the upper layer of the soil; however, this infiltrated water would be limited in recharging the aquifer due to the soils' saturated hydraulic conductivity below the extent of the macropores. The spatiotemporal resolution of the rainfall and ET could potentially have a large impact on the catchment response, particularly where short intense rainfall events lead to flashy streamflow responses, which would not be captured using the average daily rainfall. With respect to these assumptions, it is still expected that increased complexity of inputs would lead to at least the same or greater spatiotemporal variation in the different flow generation mechanisms. It is not expected that increased complexity would yield more homogeneous responses in in-stream and overland flow generation processes, although this is clearly yet to be tested. Furthermore, the influence of surface flow travel times, flow impediments, and flow depletion processes are still important with respect to spatiotemporal variability of contributing flow generation processes.

### 5.5. Evaluation of HMC Method Implementation

[70] The subtimed scheme of the HMC method is an important improvement which allowed application to more complex problems than those studied in *Partington et al*. [2011, 2012] and *Li et al*. [2013]. The subtimed scheme was necessary in both of the models, significantly reducing the number of flow solution time steps that would have been required with the previously developed HMC method (by $10^6$ in the catchment year-long simulation). The subtimed scheme allowed the adaptive time stepping scheme of the flow solution to perform as normal without tight restrictions on the maximum time step. Complementary to this improvement, the stability constraints used in the improved HMC method were able to ensure stability of the cells in the simulations. The reset fractions resulting from cells that were reset when they met the criteria outlined in section 3.3.3, highlighted areas that were of little interest with respect to overland flow generation processes. The reduction of active cells allowed faster computation and highlighted areas of little activity with respect to flow generation processes, which is reflected in the spatial distribution of the reset fraction (Figures 6, 7, and 11) and in the contributing fraction of flow from reset cells.

## 6. Conclusions

[71] In this paper, an improved Hydraulic Mixing-Cell (HMC) method was developed that enables both active and contributing processes to be obtained from the outputs of Integrated Surface-Subsurface Hydrological Models (ISSHM), thereby enabling streamflow generation processes to be identified for catchments that include significant storage, travel times, and losses. Specifically, the following improvements to the HMC method were made: (1) accounting for overland flow generation mechanisms, (2) implementing a subtimed scheme, and (3) implementing HMC stability constraints.

[72] This improved HMC approach was applied to two virtual experiments based on the Lestenbach catchment and a

wetland typical of the catchment, which enabled (i) separation of simulated streamflow hydrographs into their constituent in-stream and overland flow generation mechanisms, (ii) quantification of the spatial and temporal variability for in-stream and overland flow generation mechanisms at contrasting spatial and temporal scales, and (iii) quantification of the degree to which the active and contributing processes differ within the catchment model, leading to an improved understanding of simulated streamflow generation processes. The application of the HMC method in this study is a promising first step in the refinement of the method; however, as discussed in the model limitations, the catchment model would benefit from some improvements. Further development of the catchment model by further calibration using additional hydrometric data will serve to improve the veracity of the model for quantifying spatiotemporal variability within the Lehstenbach catchment. Furthermore, investigation into the influence of the no flow subsurface boundary conditions used and the areal mesh discretization would also help to make the catchment model more representative of the Lehstenbach catchment.

[73] Further development of the HMC method is recommended by greater subdivision of the rainfall driven overland flow generation mechanisms into saturation excess and infiltration excess. It would be extremely useful to also develop an automatic definition of the stream based on flow depth, velocity, and direction. In addition, the HMC method should be further expanded to track flow in the subsurface, which would allow tracking of other flow domains, for example, from macropores and fractures. Extension to the subsurface would also allow identification of the source areas of groundwater discharging to the surface. The inclusion of time stamps to the HMC fractions would also improve the HMC method, and allow analysis into event and preevent water contributions.

[74] The composition of streamflow with respect to the different surface runoff generating processes entails important information on runoff processes and mechanisms during large rainfall events and during dry periods. The methodology presented here provides a tool to decipher and deconvolute the integrated streamflow signal using numerical models. This improves assessment of catchment functioning within the "hypothetical reality" of the model. This is an important aspect of the HMC method when applied to physically distributed models that have no a priori assumption of flow generation processes. Use of the HMC method provides a necessary assessment of whether or not a catchment model behaves in the way desired, or more importantly, the way the catchment processes are conceptualized. In that sense, it is useful for a "soft calibration" based on understanding of catchment functioning from field observations. This can only serve to strengthen the relatively small arsenal of tools currently available for analyzing catchment models.

[75] **Acknowledgments.** The authors gratefully acknowledge Pascal Goderniaux and two anonymous reviewers whose reviews greatly improved the manuscript. The authors also gratefully acknowledge the assistance of Grace Lin in developing figures for the manuscript. This work is supported by the Australian Research Council through its Linkage scheme and the South Australian Department for Water as the industry partner under grant LP0668808. Parts of this research were funded by the Swiss National Foundation, Ambizione grant PZ00P2_126415. The views expressed in this paper are solely those of the authors.

## References

Ambroise, B. (2004), Variable 'active' versus 'contributing' areas or periods: A necessary distinction, *Hydrol. Processes*, *18*, 1149–1155, doi:10.1002/hyp.5536.

Bishop, K., J. Seibert, S. Köhler, and H. Laudon (2004), Resolving the double paradox of rapidly mobilized old water with highly variable responses in runoff chemistry, *Hydrol. Processes*, *18*, 185–189, doi:10.1002/hyp.5209.

Brunner, P., and C. T. Simmons (2012), HydeoGeoSphere: A fully integrated physically based hydrological model, *Ground Water*, *50*(2), 170–176, doi:10.1111/j.1745-6584.2011.00882.x.

Brunner, P., P. G. Cook, and C. T. Simmons (2009), Hydrogeologic controls on disconnection between surface water and groundwater, *Water Resour. Res.*, *45*, W01422, doi:10.1029/2008WR006953.

Campana, M. E., and E. S. Simpson (1984), Groundwater residence times and recharge rates using a discrete-state compartment model and C-14 data, *J. Hydrol.*, *72*, 171–185, doi:10.1016/0022-1694(84)90190-2.

Camporese, M., C. Paniconi, M. Putti, and S. Orlandini (2010), Surface-subsurface flow modeling with path-based runoff routing, boundary condition-based coupling, and assimilation of multisource observation data, *Water Resour. Res.*, *46*, W02512, doi:10.1029/2008WR007536.

Carle, S. F., and G. E. Fogg (1996), Transition probability-based indicator geostatistics, *Math. Geol.*, *28*(4), 453–476, doi:10.1007/BF02083656.

Ebel, B. A., and K. Loague (2006), Physics-based hydrologic-response simulation: Seeing through the fog of equifinality, *Hydrol. Processes*, *20*(13), 2887–2900, doi:10.1002/hyp.6388.

Ebel, B. A., K. Loague, D. R. Montgomery, and W. E. Dietrich (2008), Physics-based continuous simulation of long-term near-surface hydrologic response for the Coos Bay experimental catchment, *Water Resour. Res.*, *44*, W07417, doi:10.1029/2007WR006442.

Fleckenstein, J. H., S. Krause, D. M. Hannah, and F. Boano (2010), Groundwater-surface water interactions: New methods and models to improve understanding of processes and dynamics, *Adv. Water Resour.*, *33*(11), 1291–1295, doi:10.1016/j.advwatres.2010.09.011.

Frei, S., G. Lischeid, and J. H. Fleckenstein (2010), Effects of micro-topography on surface-subsurface exchange and runoff generation in a virtual riparian wetland—A modeling study, *Adv. Water Resour.*, *33*(11), 1388–1401, doi:10.1016/j.advwatres.2010.07.006.

Frei, S., K. H. Knorr, S. Peiffer, and J. H. Fleckenstein (2012), Surface micro-topography causes hot spots of biogeochemical activity in wetland systems: A virtual modeling experiment, *J. Geophys. Res.*, *117*, G00N12, doi:10.1029/2012JG002012.

Gaukroger, A. M., and A. D. Werner (2011), On the Panday and Huyakorn surface-subsurface hydrology test case: Analysis of internal flow dynamics, *Hydrol. Processes*, *25*(13), 2085–2093, doi:10.1002/hyp.7959.

Gerstberger, P. (2001), Waldökosystemforschung in Nordbayern, Die Bitök-Untersuchungsflächen im Fichtelgebirge und Steigerwald, in *Bayreuther Forum Ökologie, edited by BITÖ K, B. I. f. T. Ö., BITÖK*, 193 p., Bayreuther Inst. für Terr. Ökosystemforschung, Bayreuth, Germany.

Goderniaux, P., S. Brouyere, H. J. Fowler, S. Blekinsop, R. Therrien, P. Orban, and A. Dassargues (2009), Large scale surface-subsurface hydrological model to assess climate change impacts on groundwater reserves, *J. Hydrol.*, *373*, 122–138, doi:10.1016/j.jhydrol.2009.04.017.

Goderniaux, P., S. Brouyère, S. Blenkinsop, A. Burton, H. J. Fowler, P. Orban, and A. Dassargues (2011), Modeling climate change impacts on groundwater resources using transient stochastic climatic scenarios, *Water Resour. Res.*, *47*, W12516, doi:10.1029/2010WR010082.

Hauck, A. (1999), Hydrological charakterization of the Lehstenbach catchment, diploma thesis, Dep. of Ecol. Modell., Univ. Bayreuth, Bayreuth, Germany.

HydroGeoLogic Inc. (2006), MODHMS: A Comprehensive MODFLOW Based Hydrologic Modeling System, Version 3.0, Code Documentation and User's Guide, HydroGeoLogic Inc., Herndon, Va.

Ivanov, V. Y., E. R. Vivoni, R. L. Bras, and D. Entekhabi (2004), Catchment hydrologic response with a fully distributed triangulated irregular network model, *Water Resour. Res.*, *40*, W11102, doi:10.1029/2004WR003218.

Jacks, G., and A. C. Norrström (2004), Hydrochemistry and hydrology of forest riparian wetlands, *For. Ecol. Manage.*, *196*(2–3), 187–197, doi:10.1016/j.foreco.2004.01.055.

Kampf, S. K., and S. J. Burges (2007), A framework for classifying and comparing distributed hillslope and catchment hydrologic models, *Water Resour. Res.*, *43*, W05423, doi:10.1029/2006WR005370.

Knorr, K. H., B. Glaser, and C. Blodau (2008), Fluxes and C-13 isotopic composition of dissolved carbon and pathways of methanogenesis in a fen soil exposed to experimental drought, *Biogeosciences*, *5*, 1457–1473.

Kollet, S. J., and R. M. Maxwell (2006), Integrated surface-groundwater flow modeling: A free-surface overland flow boundary condition in a parallel groundwater flow model, *Adv. Water Resour.*, *29*(7), 945–958, doi:10.1016/j.advwatres.2005.08.006.

Kristensen, K., and S. Jensen (1975), A model for estimating actual evapotranspiration from potential evapotranspiration, *Nord. Hydrol.*, *6*(3), 170–188, doi:10.2166/nh.1975.011.

Kruse, J., B. Lennartz, and P. Leinweber (2008), A modified method for measuring saturated hydraulic conductivity and anisotropy of fen peat samples, *Wetlands*, *28*(2), 527–531, doi:10.1672/07-153.1.

Li, L., H. R. Maier, M. F. Lambert, C. T. Simmons, and D. Partington (2013), Framework for assessing and improving the performance of recursive digital filters for baseflow estimation with application to the Lyne and Hollick filter, *Environ. Modell. Software*, *41*, 163–175, doi:10.1016/j.envsoft.2012.11.009.

Li, Q., A. J. A. Unger, E. A. Sudicky, D. Kassenaar, E. J. Wexler, and S. Shikaze (2008), Simulating the multi-seasonal response of a large scale watershed with a 3D physically-based hydrologic model, *J. Hydrol.*, *357*, 317–336, doi:10.1016/j.jhydrol.2008.05.024.

Liggett, J. E., A. D. Werner, and C. T. Simmons (2012), Influence of the first-order exchange coefficient on simulation of coupled surface-subsurface flow, *J. Hydrol.*, *414–415*, 503–515, doi:10.1016/j.jhydrol.2011.11.028.

Lischeid, G., A. Kolb, C. Alewell, and S. Paul (2007), Impact of redox and transport processes in a riparian wetland on stream water quality in the Fichtelgebirge region, southern Germany, *Hydrol. Processes*, *21*(1), 123–132, doi:10.1002/hyp.6227.

Lischeid, G., A. Kolb, and C. Alewell (2002), Apparent translatory flow in groundwater recharge and runoff generation, *J. Hydrol.*, *265*(1–4), 195–211, doi:10.1016/S0022–1694(02)00108-7.

Loague, K., and J. E. Vanderkwaak, (2002), Simulating hydrological response for the R-5 catchment: Comparison of two models and the impact of roads, *Hydrol. Processes*, *16*, 1015–1032, doi:10.1002/hyp.316.

Maxwell, R. M., and S. J. Kollet (2008), Quantifying the effects of three-dimensional subsurface heterogeneity on Hortonian runoff processes using a coupled numerical, stochastic approach, *Adv. Water Resour.*, *31*, 807–817, doi:10.1016/j.advwatres.2008.01.020.

Mirus, B. B., B. A. Ebel, C. S. Heppner, and K. Loague (2011a), Assessing the detail needed to capture rainfall-runoff dynamics with physics-based hydrologic response simulation, *Water Resour. Res.*, *47*, W00H10, doi:10.1029/2010WR009906.

Mirus, B. B., K. Loague, N. C. Cristea, S. J. Burges, and S. K. Kampf (2011b), A synthetic-hydrologic response dataset, *Hydrol. Processes*, *25*(23), 3688–3692, doi:10.1002/hyp.8185.

Panday, S., and P. S. Huyakorn (2004), A fully coupled physically-based spatially-distributed model for evaluating surface/subsurface flow, *Adv. Water Resour.*, *27*, 361–382, doi:10.1016/j.advwatres.2004.02.016.

Park, Y.-J., E. A. Sudicky, A. E. Brookfield, and J. P. Jones (2011), Hydrologic response of catchments to precipitation: Quantification of mechanical carriers and origins of water, *Water Resour. Res.*, *47*, W12515, doi:10.1029/2011WR010075.

Partington, D., P. Brunner, C. T. Simmons, R. Therrien, A. D. Werner, G. C. Dandy, and H. R. Maier (2011), A hydraulic mixing-cell method to quantify the groundwater component of streamflow within spatially distributed fully integrated surface water—Groundwater flow models, *Environ. Modell. Software*, *26*, 886–898, doi:10.1016/j.envsoft.2011.02.007.

Partington, D., P. Brunner, C. T. Simmons, A. D. Werner, R. Therrien, H. R. Maier, and G. C. Dandy (2012), Evaluation of outputs from automated baseflow separation methods against simulated baseflow from a physically based, surface water-groundwater flow model, *J. Hydrol.*, 458–459, 28–39, doi:10.1016/j.jhydrol.2012.06.029.

Price, J. S., R. G. McLaren, and D. L. Rudolph (2010), Landscape restoration after oil sands mining: Conceptual design and hydrological modelling for fen reconstruction, *Int. J. Min. Reclam. Environ.*, *24*(2),109–123, doi:10.1080/17480930902955724.

Schlotzhauer, S. M., and J. S. Price (1999), Soil water flow dynamics in a managed cutover peat field, Quebec: Field and laboratory investigations, *Water Resour. Res.*, *35*(12), 3675–3683, doi:10.1029/1999WR900126.

Sebben, M. L., A. D. Werner, J. E. Liggett, D. Partington, and C. T. Simmons (2013), On the testing of fully integrated surface-subsurface hydrological models, *Hydrol. Process.*, *27*, 1276–1285, doi:10.1002/hyp.9630.

Shen, C., and M. S. Phanikumar (2010), A process-based, distributed hydrologic model based on a large-scale method for surface-subsurface coupling, *Adv. Water Resour.*, *33*, 1524–1541, doi:10.1016/j.advwatres.2010.09.002.

Shen, H. W., and P. Julien (1993), Erosion and sediment transport, in *Handbook of Hydrology*, edited by D. R. Maidment, pp. 12.1–12.61, McGraw-Hill, New York.

Sophocleous, M. (2002), Interactions between groundwater and surface water: The state of the science, *Hydrogeol. J.*, *10*, 52–67, doi:10.1007/s10040-001-0170-8.

Therrien, R., R. G. McLarren, E. A. Sudicky, and S. M. Panday (2009), *Hydro-GeoSphere, A Three-dimensional Numerical Model Describing Fully-integrated Subsurface and Surface Flow and Solute Transport Groundwater*, Simul. Group, Univ. of Waterloo, Waterloo, Ont., Canada.

Tromp-van Meerveld, H. J., and J. J. McDonnell (2006), Threshold relations in subsurface stormflow: 2. The fill and spill hypothesis, *Water Resour. Res.*, *42*, W02411, doi:10.1029/2004WR003800.

van Genuchten, M. T. (1980), A closed-form equation for predicting the hydraulic conductivity of unsaturated soils, *Soil Sci. Soc. Am. J.*, *44*, 892–898.

VanderKwaak, J. E. (1999), Numerical simulation of flow and chemical transport in integrated surface-subsurface hydrologic systems. PhD Dissertation, University of Waterloo, Waterloo.

Vivoni, E. R., D. Entekhabi, R. L. Bras, and V. Y. Ivanov (2007), Controls on runoff generation and scale-dependence in a distributed hydrological model, *Hydrol. Earth Syst. Sci.*, *11*, 1683–1701.

Werb, S. (2009), Simulation der hydrologischen Dynamik im Einzugsgebiet des Lehstenbachs mit dem physikalisch begründeten Modell Hydro-GeoSphere, diploma thesis, Dep. of Hydrol., Univ. of Bayreuth, Bayreuth, Germany.

Wigmosta, M. S., L. W. Vail, and D. P. Lettenmaier (1994), A distributed hydrology vegetation model for complex terrain, *Water Resour. Res.*, *30*(6), 1665–1679, doi:10.1029/94WR00436.

Winter, T. C. (1999), Relation of streams, lakes, and wetlands to groundwater flow systems, *Hydrogeol. J.*, *7*(1), 28–45, doi:10.1007/s100400050178.